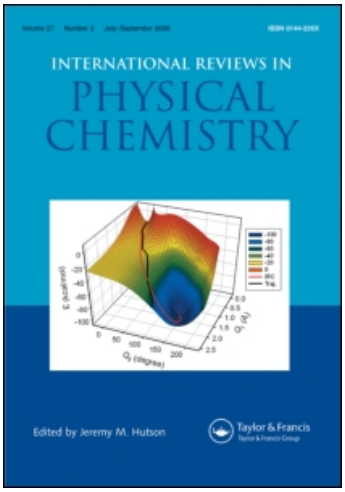

International Reviews in Physical Chemistry
Publication details, including instructions for authors and subscription information:
http://www.informaworld.com/smpp/title~content=t713724383

Structure and dynamics of quantum clusters

K. Birgitta Whaley[a]
[a] Department of Chemistry, University of California, Berkeley, CA, USA

To cite this Article Whaley, K. Birgitta(1994) 'Structure and dynamics of quantum clusters', International Reviews in Physical Chemistry, 13: 1, 41 — 84
To link to this Article: DOI: 10.1080/01442359409353290
URL: http://dx.doi.org/10.1080/01442359409353290

INTERNATIONAL REVIEWS IN PHYSICAL CHEMISTRY, 1994, VOL. 13, NO. 1, 41–84

Structure and dynamics of quantum clusters

by K. BIRGITTA WHALEY
Department of Chemistry, University of California,
Berkeley, CA 94720, USA

Quantum clusters are van der Waals aggregates of light atomic and molecular species whose behaviour is dominated by quantum delocalization and exchange effects. We summarize here recent theoretical and experimental studies of helium and molecular hydrogen clusters, focusing primarily on techniques developed to address the quantum nature of these systems. Indicators of superfluid behaviour are discussed, as well as the use of molecular probe species to study structural and dynamical properties.

1. Introduction

van der Waals bonded clusters of the lightest chemical species, namely helium, H_2 and their isotopic analogues, constitute a class of clusters with unique and unusual properties. Their low mass and weak binding cause them to be extensively delocalized even in their ground states. Both structural and dynamical properties will be influenced by the large quantum effects. Quantum-statistical effects may also be important for the pure clusters. This is most obvious for the helium isotopes, for which large differences between the Fermi and Bose systems are known in the bulk, but is also possible for molecular H_2 in selected spin and rotational states. Classical dynamical studies of the type carried out extensively in past years for heavier rare-gas clusters cannot address these issues. To achieve any realistic quantitative understanding of these clusters, it is necessary to embark on a fully quantum-mechanical description. In general, for clusters ranging from size $N=2$ to $\approx 10^5$, this is a task comparable in magnitude and in difficulty with the electronic structure problem. There are, however, important differences between the two problems. For clusters of ^{4}He and of H_2 ($J=0$), the Bose character requires a wavefunction fully symmetric instead of antisymmetric with respect to pair permutations. The lack of a central attractive nucleus means that, in the absence of impurities, the cluster wavefunction is determined solely by the interhelium interactions, while the electronic structure solutions are dependent on both electron–electron and electron–nucleus interactions. The very different nature of the van der Waals from the Coulomb potential makes both the detailed solutions and the energy scales involved very different, although for quantum clusters one can often start with techniques similar to those used for electronic structure.

Both of the helium species, ^3He_N and ^4He_N, are of interest from a physical point of view and both can be made at low temperatures, either as free clusters in molecular beam machines (Gspann and Vollmar 1978, 1980, Buchenau *et al.* 1990, Goyal *et al.* 1992a) or embedded in metallic matrices (Syskakis *et al.* 1985, 1990). Of physical interest are both the structural and the energy effects of the different Fermi and Bose statistics, as well as the finite-size scaling of collective behaviour, in particular of the superfluid state. The superfluid phase in bulk ^{4}He is accessed below about 2 K while, in bulk ^{3}He where pairing is required, the superfluid transition is at about 3 mK. Since the superfluid transition is expected to be depressed in a finite-size system (Ginsburg and Sobyanin 1976) the experimental conditions required to access superfluid clusters of ^{3}He

0144–235X/94 $10·00

are far more extreme than for superfluid clusters of the Bose isotope ^{4}He. Thus, while there is good evidence for the superfluid transition in finite bubbles of ^{4}He enclosed in a solid matrix (Syskakis *et al.* 1985), the analogous experiment with ^{3}He has proved problematic (Syskakis *et al.* 1990). In the free clusters formed in molecular beams which constitute the focus of this review, internal temperatures of the order of $T \leqslant 0{\cdot}4$ K are estimated (Buchenau *et al.* 1990). This may well allow superfluid states to be accessed for ^{4}He, but not for ^{3}He. Since a large part of the chemical interest derives from the possibility of unusual quantum solvent effects on embedded or scattered species due to superfluid characteristics of the clusters, this essential difference means that the Bose clusters of ^{4}He are of greater interest from a chemical point of view.

Superfluid clusters offer an intriguing environment for low-temperature chemistry. In the bulk, superfluidity is accompanied by large thermal conductivities, resulting in virtually instantaneous heat dissipation from local sources, and in very weak temperature gradients. If this feature holds also in a cluster of ^{4}He, it could be utilized to study energy transfer and chemical reactions under single-collision conditions, by scattering from embedded molecules. Very fast energy transfer to the quantum 'solvent' from the collision partners would strongly influence the low-temperature branching ratios. Evidence for such fast energy transfer has been seen recently in the formation of metastable solid phases of impurity atoms (nitrogen and neon) solvated by helium in bulk superfluid He II (Gordon *et al.* 1989). For large molecules with complicated branching patterns, the resulting simplification of the collision outcome would allow access to the state-to-state dynamics of very large systems and also possibly provide a new and useful route to the study of intramolecular energy redistribution.

Clusters of molecular hydrogen present additional, rather novel questions about quantum effects in low-temperature finite aggregates. In particular, the nature of their structure, that is solid or liquid, and the possibility of superfluidity in a cluster for a species which has no bulk superfluid state. There is no superfluid state in bulk H_2 because it has a triple point at 13·6 K (Weast 1981) below which only the solid and gas states are found, while the Bose–Einstein condensation temperature, which serves as an order-of-magnitude upper estimate of the superfluid transition, is predicted to be at $T = 6{\cdot}6$ K for para-H_2 (Ginsburg and Sobyanin 1972), compared with $T = 3{\cdot}2$ K for ^{4}He. Nevertheless, while finite, this is a relatively small temperature difference, and as a consequence there has been considerable effort expended over the years in trying to supercool bulk liquid H_2 below the triple point to access a new superfluid (Maris *et al.* 1983). Since H_2 exists in both the para ($I = 0$; compound boson) and ortho ($I = 1$; compound fermion) state, the possibility exists of a whole new set of superfluids. Specific-heat anomalies of hydrogen confined in small pores have been interpreted as yielding evidence for roton-like excitations (Brewer *et al.* 1990). However, most supercooling efforts so far failed to produce a superfluid. This is where utilization of the finite-size effects endemic to a cluster may have dramatic effects. It is well known and has been documented both experimentally and theoretically for a number of homonuclear clusters that freezing temperatures are lowered in finite-size systems (Borel 1981, Buffat and Borel 1976, Beck *et al.* 1989, Castro *et al.* 1990, Ercolessi *et al.* 1991). The extent of the maximum depression at small cluster sizes is dependent on the cohesive energy, with more weakly bound systems being susceptible to greater depression. Since $(H_2)_N$ has much less cohesive energy than the metal and semiconductor clusters for which the maximum T_m depression is about $\frac{1}{2}T_m$, the extreme scenario sketched in figure 1 becomes a possibility, namely a 'phase transition' between liquid- and solid-state clusters at zero temperature, as the cluster size N is increased.

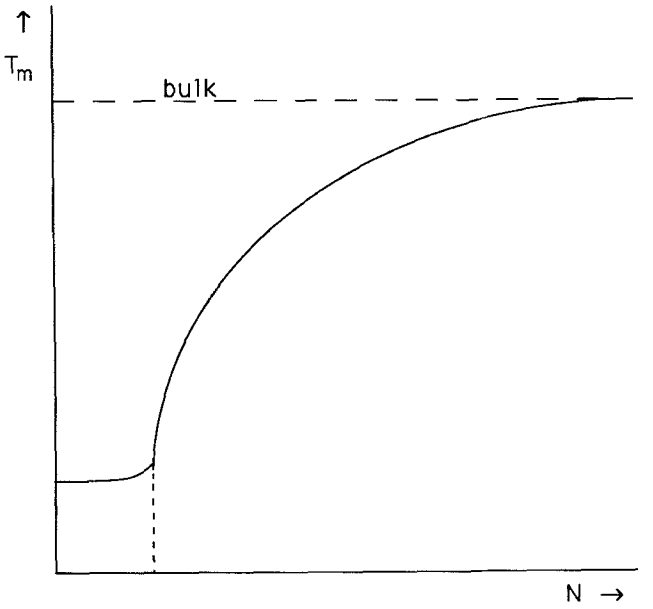

Figure 1. Schematic size dependence of the melting transition T_m in clusters as a function of size, N. The broken line shows a possible extrapolation to small sizes for particles with relatively weak cohesive forces, such as $(H_2)_N$.

Even if T_m is still finite, the general lowering of density in small clusters means that quantum delocalization effects will be larger in solid H_2 clusters than they already are in bulk solid H_2. Regardless of whether the zero-temperature structures are therefore quantum liquid or extensively delocalized quantum solids, the possibility of low-density collective behaviour defined by Bose statistics and hence of superfluid effects in finite clusters of H_2 is very real.

The final preliminary question that we wish to address is the insight into the nature of superfluidity which these clusters can offer. Despite many years of research into the properties of the liquid-helium isotopes, theoretical understanding of the superfluid state today is still largely phenomenological. Microscopic theory at the atomic level exists really only for the ground-state wavefunction and structure. While the excitation spectrum can be calculated to varying degrees of sophistication using many-body techniques, very little understanding exists of the detailed atomic dynamics in the characteristic roton states. If one can characterize a minimum-size cluster required to see these states, and one has theoretical techniques for analysis of atomic dynamics in finite clusters, then new insight into the superfluid state at the molecular level may be achieved.

The above introduction shows the various motivations for studying these very weakly bound clusters. The primary focus of this review is theoretical studies of these systems, and in §§ 3–5 we shall concentrate on these. However, since much of the theoretical work currently being done is closely coupled to experimental studies, we first give a brief overview of experimental work on clusters of helium and molecular hydrogen in the next section.

2. Experimental studies

2.1. *Helium clusters in external media*

The studies of Syskakis *et al.* (1985, 1990) of the specific heat of helium bubbles enclosed in metallic matrices were mentioned above. For ^{4}He these showed evidence of a superfluid transition at a temperature T_λ lower than the bulk value of 2·017 K, and a rounding of the specific-heat lambda discontinuity. Qualitative agreement was seen with the Ginzburg–Landau–Pitaevskii mean-field scaling arguments of Mamaladze (Ginzburg and Sobyanin 1976). For ^{3}He the lowest temperatures reached were about 15 mK; no evidence of transition to the superfluid phase was seen (Syskakis *et al.* 1990).

The formation of metastable solid phases of solvated impurity atoms in bulk He II has been observed by Gordon *et al.* (1989, 1993). These solid phases appear to consist of clusters of solvated impurity atoms stabilized by at least one layer of helium, which are decomposed on heating. Atomic nitrogen is thereby stabilized against radiative recombination at low temperatures ($T < 8$ K). Strong localization of the helium is invoked to account for the stability of the crystalline cluster phase. This may be similar to the solidification of helium believed to occur in the formation of 'snowballs', which are charged aggregates of 50–100 helium atoms surrounding impurity ions in bulk liquid helium (Schwartz 1975).

2.2. *Free helium clusters*

Free helium clusters were first formed in molecular-beam expansions by Becker *et al.* (1961) and atomic scattering as well as electronic excitation studies were subsequently carried out on very large clusters of both ^{3}He and ^{4}He in a series of experiments by Gspann and co-workers (Gspann and Vollmar 1978, 1980, Gspann 1981a, 1982, Gspann and Ries 1985). These early studies found that atomic scattering resulted in cluster deflection and also saw fragmentation of electronically excited metastable neutrals. The second experimental phase consisted of a series of mass spectrometry studies which yielded size distributions for positively charged He_N^+ (van Deursen and Reuss 1975, Stephens and King 1983, Buchenau *et al.* 1985, 1986, 1990). Stephens and King reported magic numbers for small N but no evidence of these was seen in other studies. Buchenau *et al.* (1990) used a time-of-flight (TOF) method to show that several different kinds of cluster ion are formed. They suggested that fragmentation of the adiabatically expanding fluid helium provides an additional source of neutral clusters which have velocity and, perhaps, also internal state distributions differing from those formed by condensation. These mass spectrometry studies were all limited to ionic fragment sizes of $N \leqslant 160$, and estimates of the original neutral sizes had to be made indirectly, from consideration of the expansion conditions. Such estimates gave $N \approx 10^4$ for neutral He_N (Buchenau *et al.* 1990). Recently, Jiang and Northby (1992) have developed a stopping potential energy analysis which extends the range of sizes for ionized He_N^+ to $N \approx 10^5$, and which can also measure mass distributions of negatively charged clusters. Such experiments show an exponentially decaying high-mass distribution for $N > 100$ and appear to confirm the hypothesis of two modes of cluster formation: fragmentation and condensation. The negative-ion distributions appear to have a size threshold of $N \approx 10^5$, which is consistent with the bounds placed by the prior experimental electron attachment study of Gspann (1991), as well as with the theoretical predictions of Krishna and Whaley (1988).

Atomic and molecular scattering from helium clusters was orginally suggested as a direct probe of superfluidity. Analysis of such experiments proved problematic for many years (Gspann 1982), until it was discovered that most species are readily

absorbed by the clusters. The pick-up of species such as Cs (Gspann and Ries 1986), Xe, Ne, O_2, CO, SF_6 and a number of others have now been detected, and in some cases clustering within the helium cluster is found (Scheidemann 1989, Scheidemann *et al.* 1990a, b). Generally, such absorption is consistent with a liquid structure. Detailed study of the pick-up efficiency on the cluster formation conditions has provided interesting systematic features: in particular, that clusters formed in expansions passing near the critical point are most efficient in capturing foreign species (Scheidemann *et al.* 1990b). Lewerenz *et al.* (1993) have recently used the measurement of cluster deflections due to momentum transfer from an impinging atom or molecule to measure the size of the neutrals directly. Attention has now shifted to treating the foreign species as atomic or molecular probes of the cluster environment. Recently Goyal *et al.* (1992a) have obtained the first spectroscopic measurements on such a foreign molecule, with the measurement of the vibrational spectrum of SF_6. They see a red shift and a splitting of the triply degenerate ν_3 mode which is tentatively ascribed to the SF_6 sitting in an asymmetric environment such as at the cluster surface. Dimer absorptions are also seen, with little red shifts relative to their gas-phase values. Infrared spectra have also been measured for SiF_4, and for complexes of heavier rare-gas atoms with SF_6 in He_N (Schutt 1992). Comparison with theoretical studies of impurities will be made in § 3.3. Mass spectrometry methods are now being used to address the reactions of He^+ with impurities such as SF_6 inside He_N (Scheidemann *et al.* 1993). While still in its early stages, the impurity probe approach is capable of yielding direct information on structural and dynamical properties of the clusters and bears considerable promise for the future, particularly when combined with theoretical analysis.

2.3. *Molecular hydrogen clusters*

In the first experimental studies of these clusters, Maris *et al.* (1983) attempted to supercool liquid H_2 in droplets levitated in pressurized ^4He. Temperatures of 10·6 K were attained, not low enough to reach a superfluid state. Subsequently Knuth *et al.* (1990) demonstrated the formation of free clusters of n-H_2 in a molecular beam expansion, reaching estimated temperatures of about 6 K. Goyal *et al.* (1992b) and Schutt (1992) have recently obtained the infrared spectrum of SF_6 in clusters of both n-H_2 and n-D_2 with $N \approx 1000$. Estimated temperatures are also about 6 K, and it is not clear whether under these conditions the clusters are solid like or liquid like. Both monomer and dimer red-shifted absorptions of the SF_6 ν_3 mode are detected but, in contrast with the situation in He_N, no splitting of the monomer absorption is seen. The magnitudes of the red shifts are larger than in helium. These spectra are consistent with the fact that the SF_6 is solvated at the centre of the hydrogen clusters, in contrast with the conclusions reached for helium.

3. Theory: overview and ground-state studies

3.1. *Overview*

In order to achieve an understanding of the way in which superfluid effects scale in clusters, both ground- and excited-state information is required. As in the bulk, superfluidity can be approached from two different viewpoints. The first is consideration of the spectrum of elementary excitations out of the ground state and the observation of an energy gap . Since in a finite system all excitations are discretized, there is always a trivial energy gap. One has to look instead in detail at the finite-size scaling of the roton excitations characteristic of the superfluid state, and at the finite-size energy–momentum relationship for creation of elementary excitations. This

resembles the microscopic approach of Feynman (1954) and requires some knowledge of the ground- and low-lying excited-state wavefunctions. This microscopic approach, which is discussed in §4.2, has the useful corollary that analysis of excited-state wavefunctions may yield information on the detailed atomic dynamics in rotons for finite systems. A complementary approach, based on the phenomenological two-fluid model, is to consider the response of the system to rotation. When combined with microscopic calculation of the density matrix, this can be shown to yield microscopic expressions for the normal and superfluid fractions at finite temperatures. Calculations for clusters based on path integral evaluation of the finite-temperature density matrix are discussed in §5.2.

Both of these quantities, the elementary excitation spectrum and the superfluid fraction, are accessible to direct experimental measurement in bulk He but not in free pure ^{4}He clusters. The cluster flux obtainable in molecular-beam expansions is too weak for neutron scattering, and measurement of moments of inertia for freely rotating clusters ^4He_N is likely to remain a thought experiment. This provides therefore a strong motivation to introduce impurities to act as probes of both the elementary excitations and the response to rotation. The structural perturbations induced by such impurities in the ground state are of immediate interest, since at temperatures low enough that superfluid behaviour may be manifested, the structure is expected, just as in bulk ^{4}He (Whitlock *et al.* 1979), to be similar to the ground state. (However, free rotations of the cluster, which have no analogue in the bulk, may change this; §4.2) Accurate assessment of the energy changes induced by binding of an impurity are also needed, particularly since very few species are known to dissolve in bulk helium. Similar structural and energy information in excited states with impurities are needed, as well as a comprehensive theory for the coupling of molecular or atomic impurity excitations with the cluster modes. Ground-state studies of impurities are discussed in §3.3, and finite-temperature studies in §5.2.

A third issue for theory is the treatment of scattering from quantum clusters. This means both analysis of the propensity for absorption of neutrals, and the electronic excitation and fragmentation induced by electron bombardment. Some work has been done on both of these topics and will be summarized in §5.3. Interesting but more esoteric topics such as light scattering and very-high-energy elastic electron scattering have not yet been addressed by either theory or experiment.

In the rest of this section we describe ground-state studies. Section 4 then deals with excited states and addresses the above-outlined issues in detail. Studies of both helium and molecular hydrogen will be referred to together, classified by their focus, that is ground state, excited state, etc., rather than by the cluster make-up. Section 5 describes finite-temperature and scattering studies. We conclude with some discussion of future directions for these systems in §6.

3.2. *Ground states: quantum Monte Carlo methods*

The first applications of quantum Monte Carlo (QMC) techniques to these clusters were made by nuclear physicists who employed helium clusters as test systems in developing computational techniques for ground-state studies of nuclei. In a series of papers beginning in 1983, Pandharipande and co-workers (Pandharipande *et al.* 1983, 1986, Pieper *et al.* 1985, Lewart *et al.* 1988) showed the viability of QMC for accurate ground-state calculations, making both variational Monte Carlo (VMC) and Green function Monte Carlo (GFMC) calculations. Extensive ground-state studies of helium

and hydrogen clusters using VMC have been made by Krishna and Whaley (1990a–d, 1991a) and Barnett and Whaley (1993a) Rick *et al.* (1991b) and Rick and Doll (1992) have used VMC to also analyse the quantum effects in ground states of helium and heavier rare-gas clusters. The VMC method was recently refined and extended to deal with clusters containing impurities by Barnett and Whaley (1992). All VMC calculations have been calibrated by comparison with exact calculations, either with GFMC or, more recently, diffusion Monte Carlo (DMC) methods. DMC studies have been carried out by Krishna and Whaley (1990d), Rick *et al.* (1991a), Chin and Krotscheck (1990, 1992) and Barnett and Whaley (1993a). We now discuss the ground-state VMC literature.

3.2.1. *Variational Monte Carlo method for pure clusters*

The VMC approach to cluster ground states consists of proposing a many-body wavefunction $\psi(\mathbf{R})$ and then optimizing the parameters that it contains. Generally, one seeks a minimum in the ground-state energy:

$$\langle E\rangle = \int \psi^* \hat{H}\psi \, d\tau \Big/ \int \psi^* \psi \, d\tau. \tag{3.1}$$

Equation (3.1) may be rewritten in terms of a probability density function $p(\mathbf{R}) = \psi^*(\mathbf{R})\psi(\mathbf{R})$:

$$\langle E\rangle = \int p(\mathbf{R}) E_L(\mathbf{R}) \, d\mathbf{R} \Big/ \int p(\mathbf{R}) \, d\mathbf{R}, \tag{3.2}$$

where the local energy is given by

$$E_L(R) = \frac{\hat{H}(\mathbf{R})\psi(\mathbf{R})}{\psi(\mathbf{R})}. \tag{3.3}$$

The energy can then be computed as a finite sum over points sampled from $p(\mathbf{R})$:

$$\langle E\rangle \approx M^{-1} \sum_{i=1}^{M} E_L(\mathbf{R}_i), \tag{3.4}$$

where equality is reached as $M \to \infty$. Most workers have used the standard Metropolis walk to sample $p(\mathbf{R})$ (Pandharipande *et al.* 1986, Krishna and Whaley 1990b, d, Rick *et al.* 1991b). Barnett and Whaley (1993a) have made a detailed study of the relative efficiency of the standard 'unguided' Metropolis walk, and a walk 'guided' by ψ.

For the pure Bose species, accurate ground-state wavefunctions are given by the nodeless form

$$\psi(\mathbf{R}) = \exp\left(\sum_{i<j<N} t_2(r_{ij}) + \sum_{i<j<k<N} t_3(r_{ij}, r_{ik}) \right). \tag{3.5}$$

This generalized Jastrow form is symmetrized with respect to all pair permutations, and because of its exponential nature it is very well suited to dealing with the strongly repulsive short-range interactions. Equation (3.5) is a generalization of the most accurate ground-state variational wavefunction available for bulk liquid ^{4}He today. Some workers have introduced an additional multiplicative factor χ_1 to improve binding for larger clusters, in the form of either a product of true single-particle terms describing motion in an effective binding potential (Pandharipande *et al.* 1983, 1986, Krishna and Whaley 1990b, d, Rick *et al.* 1991b), or an implicit N-particle term describing confinement to the centre of mass (Chin and Krotscheck 1990, 1992). Several

pair correlation terms t_2 have been employed. Initially the functional form was chosen to model particular physical types of correlation (Pandharipande *et al.* 1986, Krishna and Whaley 1990b, d, Rick *et al.* 1991b). Recently Barnett and Whaley (1992) have had considerable success with fitting $\chi_2(r)=\exp[t_2(r)]$ to the bound state of the HeH_2 van der Waals dimer. They have also explored parametrizing the short-range part of χ_2 in terms of the pair potential, in order to reduce large fluctuations in the local energy at small separation (Barnett and Whaley 1993a). Less work has been done on the triplet correlation term t_3, and all workers so far have used the same functional form developed for bulk liquid helium (Usmani *et al.* 1982).

Barnett and Whaley (1992) have generalized these wavefunctions to incorporate impurities. When an impurity X is added which interacts isotropically with helium, equation (3.5) is multipled by

$$\chi=\prod_{i=1}^{N} f_2(r_{ix}), \tag{3.6}$$

where f_2 is also an exponential function. For anisotropic interactions such as derive from molecular impurities, f_2 becomes a function of one or more angles in addition to the distance. Three-particle correlation terms involving the impurity have also been explored (Barnett and Whaley 1993b). These wavefunctions can also be modified to allow greater localization by introducing extra 'shadow' degrees of freedom. This was first done by Krishna and Whaley (1991a) for clusters of H_2 and was subsequently generalized by Rick *et al.* (1991b) for investigation of localization in ground states of neon and argon. Finally, for the Fermi systems studied by Pandharipande *et al.* (1986) namely ^3He_N, equation (3.5) is multiplied by a Slater determinant of free-electron gas functions.

These trial wavefunctions then typically contain a total of between seven and 15 parameters, which have to be variationally optimized. Usually the expectation value of the local energy is minimized, although the variance can also be minimized to emphasize local wavefunction accuracy. Most workers have performed parameter optimization on a fixed sample of M points (equation 3.4), with intermittent updating of the sample to take account of large wavefunction changes during optimization. Several schemes have been employed for minimization, including conjugate gradient, simulated annealing and least-squares fitting. In all cases, however, hand optimization of some of or all the parameters has proved invaluable. Systematic features of optimization have been discussed by Barnett and Whaley (1993a).

The VMC energies of a range of cluster sizes are summarized in table 1 for ^4He_N, and in table 2 for $(H_2)_N$. The binding is generally very weak, with the ground-state energies $E(N)/N$ per particle increasing from $-0{\cdot}039$ K for the first bound helium system, $N=3$, to $-4{\cdot}95$ K for the largest cluster yet studied, $N=728$. The latter is still only 70% of the bulk binding energy, 7·11 K per particle (Pandharipande *et al.* 1983). ^3He_N clusters are much more weakly bound and a minimum size of $N\approx 40$ is required to achieve negative energy (Pandharipande *et al.* 1986). This is a direct consequence of the additional repulsion arising from the Pauli exclusion in the Fermi systems. For both ^4He_N and ^3He_N, with $N\geqslant 20$, ground-state energies have been fitted with the classical liquid-drop formula containing volume (E_v), surface (E_s) and curvature (E_c) terms (Pandharipande *et al.* 1986):

$$\frac{E(N)}{N}=E_v+E_s x+E_c x^2, \tag{3.7}$$

Table 1. Ground-state properties of ^4He_N: energies (E/N) per particle, r.m.s. radii $\langle R^2\rangle^{1/2}$ and unit radii r_0. Energies followed by an asterisk are computed with HFDHE2 potential (Aziz *et al.* 1979). All other values are computed with the HFD–B(HE) potential (Aziz *et al.* 1987).

N	E/N (VMC) (K)	E/N (DMC) (K)	E/N (GFMC) (K)	$\langle R^2\rangle^{1/2}$ (DMC) (Å)	r_0 (DMC) (Å)
3	−0·0415(1)[a]	−0·0443(1)[a]		6·25	5·60
	−0·0371(1)[h]	−0·0392(1)*[a]	−0·0391(1)*[b]	6·49	5·81
4	−0·1356(1)[a]	−0·11445(2)[a]	−0·1333(5)*[b]	5·07	4·13
5	−0·2502(1)[a]	−0·2678(6)[a]	−0·2514(4)*[c]	4·83	3·65
6	−0·3697(1)[j]	−0·3984(8)	−0·3735(5)*[c]	4·89	3·47
7	−0·4838(1)[d]	−0·5221(5)[a]	−0·4965(7)*[c]	4·77	3·22
14	−1·1290(7)[d]	−1·2478(12)[a]	−1·2080(40)*[c]	5·28	2·83
20	−1·510(2)[d]	−1·688(2)[a]		5·65	2·69
	−1·461(1)[h]	−1·626(2)*[a]	−1·627(3)*[b]	5·71	2·72
40	−2·430(2)[e]	−2·575(3)[e]		6·70	2·53
70	−3·043(1)[e]	−3·253(4)[e]	−3·12(4)*[b]	7·72	2·42
112	−3·476(4)[h]	−3·780(3)[a]		8·92	2·39
240	−4·192(4)[f]			10·68	2·22[g]
728	−4·95[b]			16·16	2·32[g]

[a] Barnett and Whaley (1993a).
[b] Pandharipande *et al.* (1983).
[c] Melzer and Zabolitzky (1995).
[d] Barnett and Whaley (1992).
[e] Barnett and Whaley (1993b).
[f] Krishna and Whaley (1990b).
[g] VMC value.
[h] R. N. Barnett (1992, private communication).
[j] McMahon *et al.* (1993).

Table 2. Ground-state properties of $(H_2)_N$ (McMahon and Whaley 1993), energies E/N per particle, r.m.s. radii $\langle R^2\rangle^{1/2}$ and unit radii r_0. All values are computed by VMC with the potential of Buck *et al.* (1983).

N	E/N (K)	$\langle R^2\rangle^{1/2}$ (Å)	r_0 (Å)
2	−2·155(1)	5·15	5·286
6	−11·389(5)	3·52	2·499
7	−13·013(2)	3·67	2·482
13	−19·98(1)	6·05	3·327
33	−29·75(1)	8·14	3·280

where $x = N^{-1/3}$. This enables the chemical potential to be obtained via the relation

$$\mu = \frac{dE}{dN}. \tag{3.8}$$

Lewart *et al.* (1988) have used the variational ground-state wavefunctions to obtain natural orbitals and hence to evaluate the single-particle momentum distribution and condensate fraction n_0. Simple model calculations for non-interacting bosons in a spherical box predict an increase in n_0 as the radius is decreased (Krishna and Whaley 1991b). Since the average radius generally decreases as N decreases, except for $N \leqslant 7$ (see below), this implies that n_0 should exceed the bulk value of about 0·10 in the finite interacting clusters. For $N = 70$ the non-interacting confined boson model yields $n_0 \approx 0{\cdot}26$, while Lewart *et al.* (1988) estimate that $n_0 \approx 0{\cdot}36$ from the variational ground state.

Table 2 indicates that clusters of molecular hydrogen are more strongly bound. They also show quite different structural characteristics as we now discuss. Two general structural parameters are the r.m.s. radius $\langle R_2 \rangle^{1/2}$, where R is measured from the centre of mass, and the unit radius $r_0 = (5\langle R^2 \rangle/3)^{1/2} N^{-1/3}$, which gives the volume per particle in an equivalent sphere of uniform density. For helium we quote the DMC results in table 1, for which r_0 decreases monotonically to a value close to the bulk value (2·22 Å) for $N \geqslant 100$, while $\langle R^2 \rangle^{1/2}$ shows a minimum at $N = 7$. This is consistent with the breakdown of the liquid-drop energy scaling for $N < 20$. For the very small clusters ($N \leqslant 7$), the addition of an extra atom causes a very large percentage gain in binding and a large contraction from the extremely diffuse trimer. However, this effect saturates at fairly small N because of the strongly repulsive nature of the He–He interaction and is followed by an approximately constant volume increase with each further helium addition. An interesting detail is the slight drop in $\langle R^2 \rangle^{1/2}$ at $N = 7$, implying that the $N = 7$ structure is anomalously small and compact. This may be a residual 'ghost' effect of the stability of the classical pentagonal bipyramid structure. The size reduction for $N = 7$ relative to $N = 6$ was also seen in VMC by Rick and Doll (1992). For $(H_2)_N$, $\langle R^2 \rangle^{1/2}$ has a minimum at $N = 6$ after which it monotonically increases. However, r_0 has a more complex non-monotonic behaviour, with a minimum at $N = 7$ and a maximum at $N = 13$. The behaviour of $\langle R^2 \rangle^{1/2}$ is similar to that for He_N, but the different behaviour of r_0 for $(H_2)_N$ suggests that these clusters are not described very well by pure liquid models. Nevertheless, at $N = 33$ the unit radius r_0 is still considerably higher than the bulk value at 1 atm pressure (2·09 Å), indicating a considerable amount of delocalization.

The single-particle density distributions for ^4He_N show monotonic decay from the centre, with a diffuse surface region and with the central density rising to that of bulk ^{4}He for $N \approx 200$ (figure 2). The larger clusters have an apparently uniform interior density and no statistically significant density oscillations are seen in either low- or high-resolution studies at the VMC level. However, high-resolution studies of He_3 have shown an additional central peak (figure 2 *a*) whose origin could be traced to a high weight of nearly collinear configurations by construction of conditional probability distributions (Barnett and Whaley 1992). The large weight of classically unstable configurations for this species was also noted by Rick *et al.* (1991b). The Fermi clusters ^3He_N do show some evidence for density oscillations in the interior regions, although these are reduced when the back-flow correlation term f_3 is included (Pandharipande *et al.* 1986). Generally, such density oscillations are less favourable for helium than for heavier classical systems, because of the high surface tension and low compressibility of

helium systems (Stringari and Treiner 1987). With $(H_2)_N$ the situation is very different, as is evident from figure 3. Spherical radial density distributions show pronounced structure which is consistent in all cases with some degree of hard core packing. As for the He_3 case, more detail can be obtained by constructing conditional densities or contour plots. Figure 3*b* shows a contour plot for $(H_2)_7$, which clearly indicates the presence of a nearly spherical ridge of high density. Detailed analysis shows that this is likely to be caused by a large contribution of asymmetric structures approximating the classical pentagonal bipyramid (McMahon *et al.* 1993). However, there is still a large extent of delocalization, whether we choose to refer to them as 'quantum solids' or as 'quantum liquids'. Evaluation of higher-order structural correlation functions will be required to quantify the extent of localization.

Higher-order correlations studied to date have included two-particle distributions, bond angle and dihedral angle distributions. The full anisotropic pair distribution function $g_2(\mathbf{r}_1, \mathbf{r}_2)$ (Pieper *et al.* 1985), its value from the origin, $g_2(\mathbf{0}, \mathbf{r}_2)$ (Krishna and Whaley 1990b) and the more averaged pair distribution function $p(r_{ij})$ (Barnett and Whaley 1992) for ^4He_N are seen to have typical quantum fluid oscillatory structure, with correlations which increase with increasing N. For $(H_2)_N$ the structure occurs at smaller N and is more pronounced (figure 3). The same is true for the angular correlation (Krishna and Whaley 1991a). Rick *et al.* (1991b) have made an interesting study for small clusters of the heavier rare-gas species, Ne and Ar ($N \leqslant 7$), using VMC wavefunctions with shadow coordinates. These clusters are all strongly localized and in this situation quantitative analysis of the extent of delocalization and quantum effects is possible.

3.2.2. *Exact calculations: Green function Monte Carlo and diffusion Monte Carlo methods*

VMC can yield only an upper bound to the true ground-state energy, and so it is necessary to check the accuracy, whenever possible, both of the energy and of structural features which are often more sensitive to small changes in the wavefunction. Both GFMC and DMC methods are techniques for iterating from a trial wavefunction to the ground-state wavefunction and thereby yielding exact energies. In the GFMC method the time-independent Schrödinger equation is solved in integral form, with the time-independent Green function sampled at each iteration (Kalos *et al.* 1974):

$$\psi^{(n+1)}(\mathbf{R}) = \int d\mathbf{R}'\, G(\mathbf{R}, \mathbf{R}')\psi^{(n)}(\mathbf{R}'). \tag{3.9}$$

Details of GFMC calculations for helium have been given by Kalos *et al.* (1981). DMC iterates the time-dependent Schrödinger equation in imaginary time:

$$-\hbar \frac{\partial}{\partial t}[\Phi(\mathbf{R}, t) = H(\mathbf{R})\Phi(\mathbf{R}, t), \tag{3.10}$$

with

$$H = -\sum_i D_i \nabla_i^2 + V, \tag{3.11}$$

$$D_i = \frac{\hbar^2}{2m_i}, \tag{3.12}$$

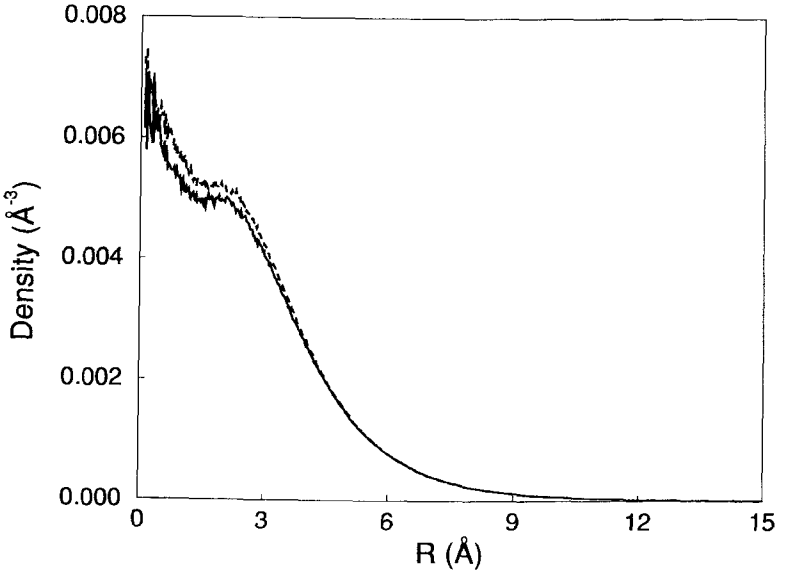

(*a*)

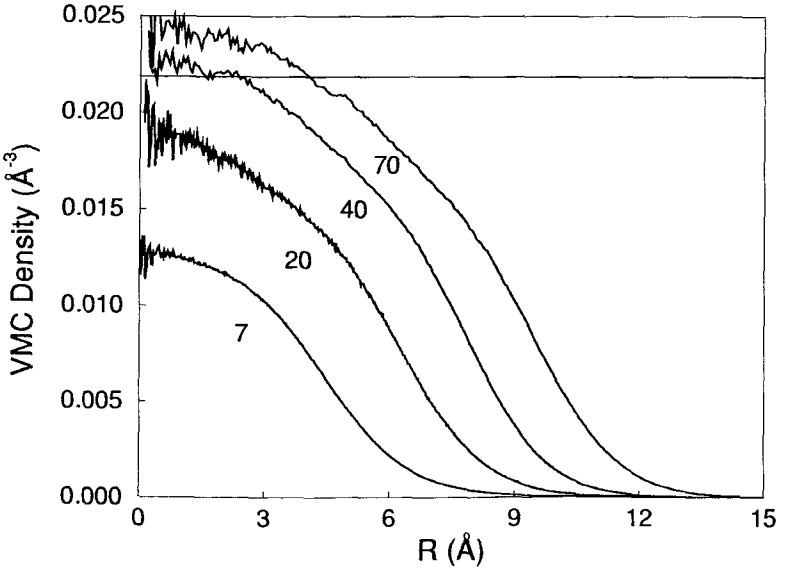

(*b*)

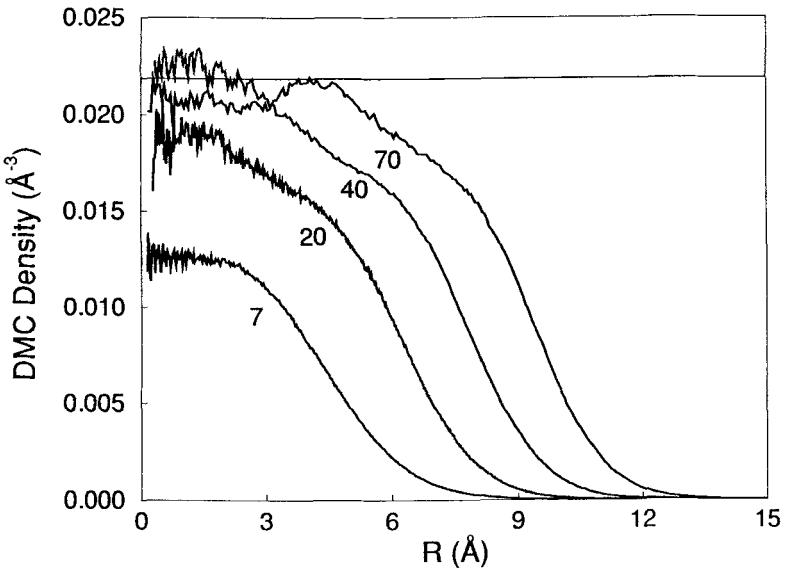

(*c*)

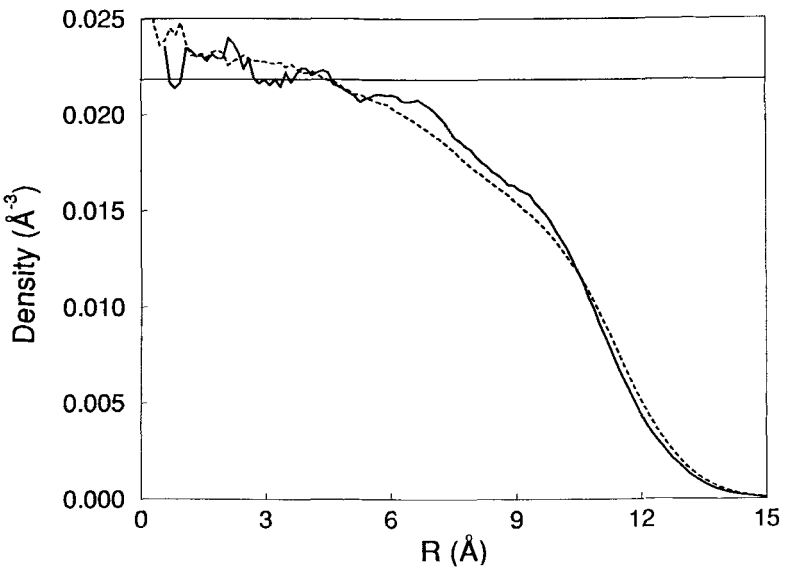

(*d*)

Figure 2. Single-particle radial density profiles for ground-state ^4He_N clusters: (*a*) $N=3$: (*b*) $N=7$, 20, 40 and 70, VMC results; (*c*) $N=7$, 20, 40 and 70, second-order DMC results; (*d*) $N=112$. ----, VMC; and ——, DMC for (*a*) and (*d*).

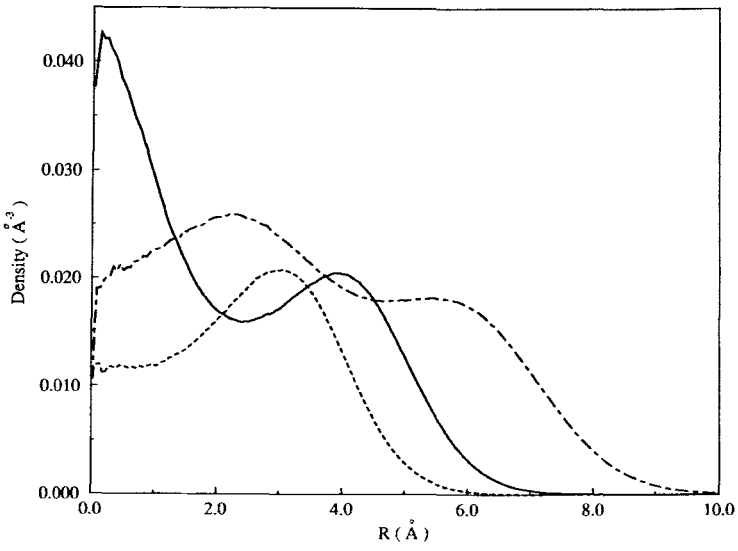

(*a*)

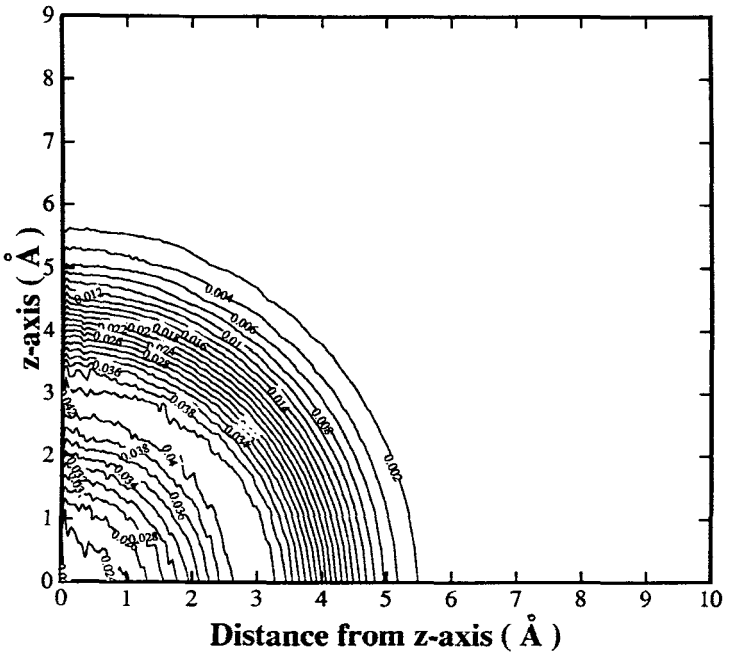

(*b*)

Figure 3. (*a*) Single-particle radial density profiles for ground state $(H_2)_N$ clusters: $N = 7$, 13 and 33; VMC results from (M. McMahon and K. B. Whaley 1993, unpublished data) (*b*) Contour plot of the density distribution function $\rho(z, r)$, where r is the two-dimensional radial coordinate in the x–y plane, for $N = 7$. For (*a*): - - -, $(H_2)_7$; —, $(H_2)_{13}$; and – · –, $(H_2)_{33}$.

until, at large t, the ground state is obtained. Iteration is accomplished by sampling a known Green function $G_a(t)$, which becomes equal to the (generally unknown) true Green function $G(t)$ for equation (3.10) as the time Δt goes to zero. That is, the large-t solution is obtained by iterating for many time steps Δt, sampling from $G_a(\Delta t) \approx G(t)$. This 'short-time' approximation necessitates that care be taken to eliminate time step bias in computed results.

Statistical error in both techniques is reduced by use of importance sampling. For DMC this is incorporated by defining new density functions

$$f(\mathbf{R}, t) = \psi(\mathbf{R})\Phi(\mathbf{R}, t), \tag{3.13}$$

for which the imaginary time-dependent equation becomes

$$-\hbar \frac{\partial}{\partial t}[f(\mathbf{R}, t) = -\sum_i D_i \nabla_i^2 f(\mathbf{R}, t) + E_L(\mathbf{R}) f(\mathbf{R}, t) + \sum_i D_i \nabla_i \cdot [f(\mathbf{R}, t)\mathbf{F}_Q(\mathbf{R})], \tag{3.14}$$

where $E_L(\mathbf{R})$ is the local energy (equation (3.3)) and $\mathbf{F}_Q(\mathbf{R}) = \nabla \ln(|\psi(\mathbf{R})|^2)$ is the 'quantum force'. Usually, ψ is a variational wavefunction chosen to approximate the ground state Φ. The ground-state energy can then be obtained from an average of the local energy over $f(\mathbf{R}, t)$. For operators A not commuting with H, such as coordinate operators, most researchers have employed the 'second-order' estimator of $\langle \Phi | A | \Phi \rangle$:

$$\langle A \rangle_s = \frac{2\langle \psi | A | \Phi \rangle}{\langle \psi | \Phi \rangle} - \frac{\langle \psi | A | \psi \rangle}{\langle \psi | \psi \rangle}. \tag{3.15}$$

Rick *et al.* (1991a) employ DMC without importance sampling. This is acceptable since the He–He interaction is bounded from below but is nevertheless less efficient than employing a trial function to bias or 'guide' the walk. This becomes more important for clusters containing impurities which cause local ordering in the surrounding helium (Barnett and Whaley 1993b). Details of DMC calculations with importance sampling for helium clusters have been discussed by Chin and Krotscheck (1992) and by Barnett and Whaley (1993a).

General energy trends of the ground states were discussed above for the VMC solutions. Agreement between converged GFMC or DMC with VMC for a range of N (table 1) shows that the variational wavefunctions of § 3.2.1 can give accurate upper bounds to the ground-state energies. Here we shall focus just on the additional information which these exact techniques provide.

^4He_N ground-state energies obtained with GFMC and DMC for selected cluster sizes are listed in table 1. The potentials used are both based on Hartrel Fock plus damped dispersion, i.e. HFD. Calculations performed with the newer He–He potential, HFD–B(HE) give energies significantly below those resulting from the older HFDHE2 potential. With the same potential, the DMC (Barnett and Whaley 1993a) and GFMC (Pandharipande *et al.* 1983) results for the same potential agree, except for the largest cluster $N = 112$, for which the DMC gives a lower energy. The GFMC calculations may have convergence difficulties for larger clusters. The DMC results of Chin and Krotscheck (1992), obtained with a different DMC algorithm and the HFDHE2 potential are consistently lower than both the GFMC and the DMC results with this potential (Barnett and Whaley 1993a). The reason for this discrepancy is unclear as it is well beyond statistical error. In the absence of convergence details for the results of Chin and Krotscheck it appears most likely that there are long-lived metastable states contributing to the time averages in the calculations of Chin and Krotscheck (1992).

Helmbrecht and Zabolitzky (1984) carried out a systematic study with GFMC for all ^4He_N clusters with $N<33$ and showed that there are no energy magic numbers corresponding to clusters of enhanced energy stability. This is consistent with extremely delocalized liquid-like structures for the pure clusters.

The structural parameters $\langle R^2\rangle^{1/2}$ and r_0 have been summarized for DMC in table 1 and the implications for the stability of the smaller clusters have been discussed above. While there are no magic numbers energetically, accurate structural studies are now showing evidence of structural compactness for certain sizes. Density profiles evaluated by DMC show some differences from the corresponding VMC profiles. Chin and Krotscheck (1990, 1992) reported a small oscillatory structure in low-resolution studies of $\rho(r)$ for ^4He_N, $N>70$, which may also be due to contributions from long-lived metastable states. Higher-resolution converged studies for He_{112} by Barnett and Whaley (1993a) show that the oscillations in the interior are within the statistical error, but that there is a small shoulder on the decay into the diffuse surface region (figure 1 *d*). Larger differences are seen between DMC and VMC calculations for heterogeneous clusters, discussed below. DMC calculations for $(H_2)_N$ also show more pronounced structure than the VMC results in figure 2 (McMahon and Whaley 1993, submitted).

3.3. *Quantum Monte Carlo studies of impurities bound to* ^4He_N

Barnett and Whaley (1992) have employed VMC and DMC to study the ground state of helium clusters containing a molecular impurity, using the wavefunctions in equations (3.5) and (3.6). Comparison of DMC with VMC calculations show that a high accuracy can be obtained by VMC when the functional form of the additional pair function χ is tailored to fit the bound-state wavefunction for the HeX dimer. The molecular impurities studied so far, H_2, D_2 and SF_6, cover a wide range of ground-state structural behaviours, which can be generally understood in terms of the different strength of the He–X interactions and of the different impurity masses.

The H_2–He van der Waals interaction is very accurately known, and the H_2He dimer possesses at least one bound state. This was therefore a natural choice for development of the VMC impurity methodology (Barnett and Whaley 1992). The ground-state energy is lowered on exchanging one helium for a H_2, as one would expect from the greater binding of He with H_2. The exchange energy, defined as

$$E_{ex}(N)=E(H_2He_{N-1})-E(He_N) \tag{3.16}$$

increases monotonically from a value of $-0{\cdot}143$ K for $N=3$, to $-1{\cdot}68$ K for $N=20$. The bulk value has been estimated to be about -20 K from density functional studies (Kürten and Ristig 1985). The ground-state structures correspond to a very delocalized H_2 which has very little perturbing influence on the helium density. Figure 4 shows the ground-state density profiles for $N=2$, 13 and 20. The helium profiles are very similar to those in the pure clusters. Despite the appearance of a peak in the H_2 density, the single H_2 species is clearly delocalized over the entire cluster. The trimer H_2He_2 is unique in having the H_2 peak at the centre, which reflects the large weight of near-collinear configurations just as in He_3. Generally, the peak occurs at an intermediate location. Detailed quantitative analysis of the H_2 distribution shows that the H_2 tends to reside at larger distances from the cluster centre for the larger clusters but nevertheless remains well within the cluster surface (Barnett and Whaley 1992). H_2He_{13} is anomalous in that a higher percentage of the H_2 lies outside the radius containing 50% of all particles. This indicates a structural robustness of the He_{13} unit, similar to that inferred for He_7 earlier, which may be associated with a 'ghost' of the

classical icosahedral structure. These studies were carried out using the isotropic H_2–He interaction potential. Incorporating the potential anisotropy gives slight increases in binding energy, but otherwise little change is seen (R. N. Barnett 1992, private communication). The situation is very different for the heavier isotope, D_2, shown in figure 5 (Barnett *et al.* 1993). The heavier isotope is considerably more localized at the centre of the cluster and has no peak in or near the surface region. This reflects the greater binding of the D_2He system. The helium distribution is now complementary to the D_2 distribution, showing a peak away from the cluster centre. Note that for D_2He_2 the central peak corresponding to nearly collinear configurations still persists, however.

The heavier impurity SF_6 possesses a stronger interaction with helium (Pack *et al.* 1984); the well depth for approach along the three symmetry axes varies from 41 to 84 K. The isotropic component of the interaction has a well depth of 62 K. Barnett and Whaley (1993b) have carried out both VMC and DMC calculations for a range of sizes and find that in the ground state the SF_6 is strongly bound in the centre of the cluster. The DMC density distributions show marked structuring of the helium in shells around the central SF_6 species, summarized in figure 6 for $N=20$, 39 and 111. This structure is very difficult to reproduce at the VMC level of calculation and confirms the importance of carrying out exact DMC calculations whenever possible to verify or to check variational results. Comparison with the bulk densities of liquid and solid helium shows that the first 'solvent shell' of helium is definitely solid, and that extensive structuring of the remaining helium occurs into liquid-like solvation shells about the SF_6. Integration of the helium density in successive shells implies that 22–23 atoms are contained in the first solvation shell, which is near to the value of 20 obtained in classical studies of $ArSF_6$ (Chartrand *et al.* 1991).

The location of the SF_6 is of considerable interest experimentally, since SF_6 attachment to He_N has recently been studied both mass spectrometrically and spectroscopically, with conflicting conclusions. Schneidemann *et al.* (1993) have performed mass spectrometry analysis of SF_6He_N. They found a large proportion of SF_6^+ in the products, leading them to conclude that the SF_6 must be located in the centre of the cluster to allow efficient quenching of SF_6^+, rather than fragmentation to SF_5^- and SF_4^+, which are the more abundant products in gas-phase ionization of SF_6. On the other hand, Goyal *et al.* (1992a, b) have recently employed the laser bolometry detection method to obtain the vibrational spectrum of SF_6 attached both to He_N and to $(H_2)_N$. They find a red shift of about $1{\cdot}5\,cm^{-1}$ and a splitting of the ν_3 monomer absorption in He_N, which is interpreted to imply that the SF_6 sits in an asymmetric environment such as at the cluster surface. For $(H_2)_N$, in contrast, no splitting of the monomer absorption is seen, which implies that the SF_6 is located in the centre here. Spectral shifts of vibrational lines are due to stretching dependence of the impurity vibration on a nearby van der Waals bonded helium or H_2. For SF_6 in argon clusters, the dominant component of this was shown by Eichenauer and LeRoy (1988) to be the instantaneous vibrational dipole–induced-dipole interaction. This electrostatic effect has been investigated for SF_6He_N by Barnett and Whaley (1993b), using the first-order perturbation theory formulation of Eichenauer and LeRoy, adapted to quantum systems. At the DMC level and employing the full anisotropic He–SF_6 interaction, this yields average red shifts of about $0{\cdot}9\,cm^{-1}$ for clusters with $N\approx 111$ and a linewidth of about $0{\cdot}3\,cm^{-1}$. No splitting of the absorption is seen, which is consistent with a centrally located impurity. However, no splitting is also predicted theoretically for the dimer, which represents an extremely asymmetric system. This is apparently due to the

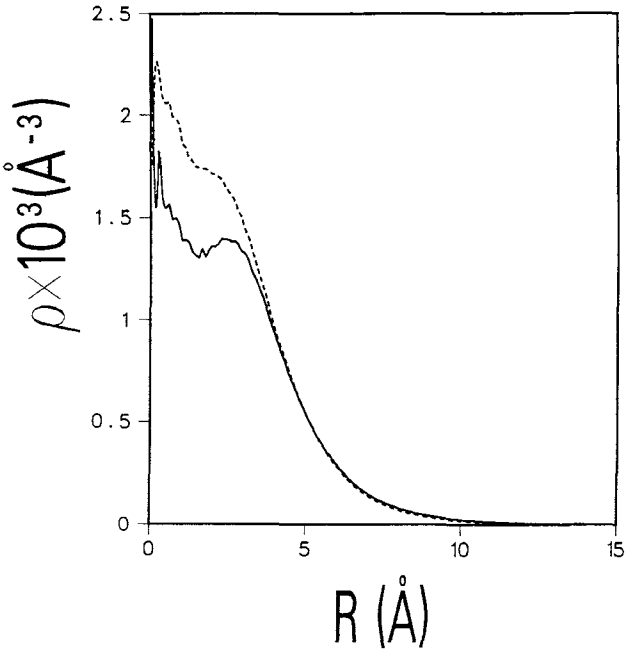

(*a*)

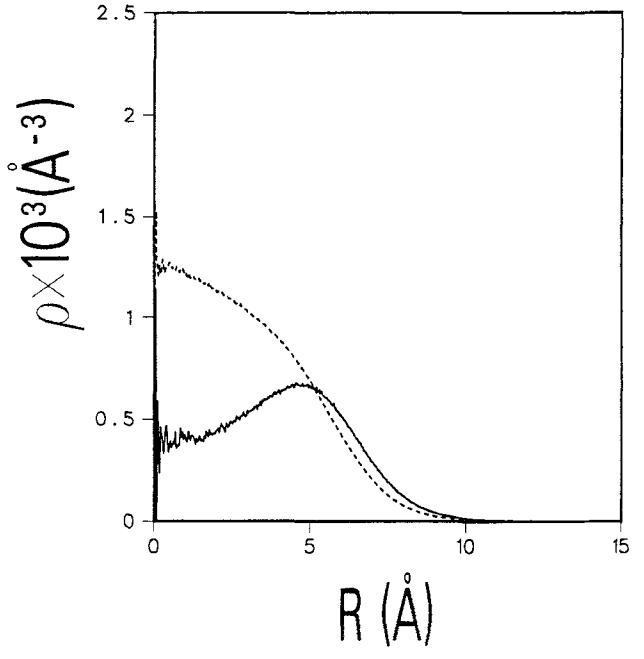

(*b*)

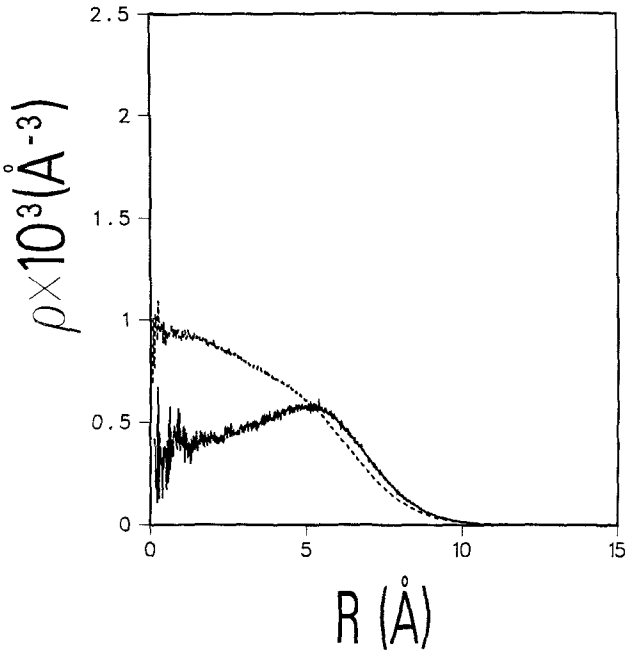

Figure 4. Single-particle radial density profiles for ground state H_2He_N clusters: (*a*) $N=2$; (*b*) $N=13$; (*c*) $N=20$. The broken and solid curves refer to helium and to H_2 respectively and are normalized to one particle per cluster in each case; VMC results. (From Barnett and Whaley 1992.)

very large zero-point delocalization. Thus, in order to obtain a splitting of the threefold-degenerate vibrational absorption in helium clusters theoretically, it may be necessary to incorporate the stretching dependence of the repulsive part of interaction potential, which is not well known. Another possible reason for the discrepancy may be that experimentally the clusters are formed in high-angular-momentum states, in which the SF_6 is located near a surface because of centrifugal forces or vortex formation. Theoretical methods of treating rotating clusters are discussed in §4.3.

Recently, Bacic *et al.* (1992) made a VMC and GFMC study of the small clusters Cl_2He_2 and Cl_2He_3, employing atom–atom pairwise Morse potentials. For these very small systems they find that the zero-point energy can be approximated by the sum of the contributions from all Cl_2He fragments and all possible He_2 fragments. Consideration of the ground-state energies of pure He_N in table 1 shows that this interesting correlation will be likely to break down for larger cluster sizes when the contribution from He–He interactions is no longer additive. There have also been several studies of atoms and molecules attached to very small clusters of ^4He_N employing non-QMC methods. Horn *et al.* (1989) made vibrational self-consistent field (SCF) studies of $XeHe_2$, and Kosloff *et al.* (1987) have used a time-dependent SCF method to analyse the dissociation of I_2He_N, $N=1$–4. The dynamics of somewhat larger I_2He_N clusters ($N=1$–9) have been analysed in a quasi-classical approach by Garcia-Vela *et al.* (1990), in a restricted geometry study. The time-dependent SCF study appeared to show a size-independent dissociation rate, while the quasi-classical calculations indicated that

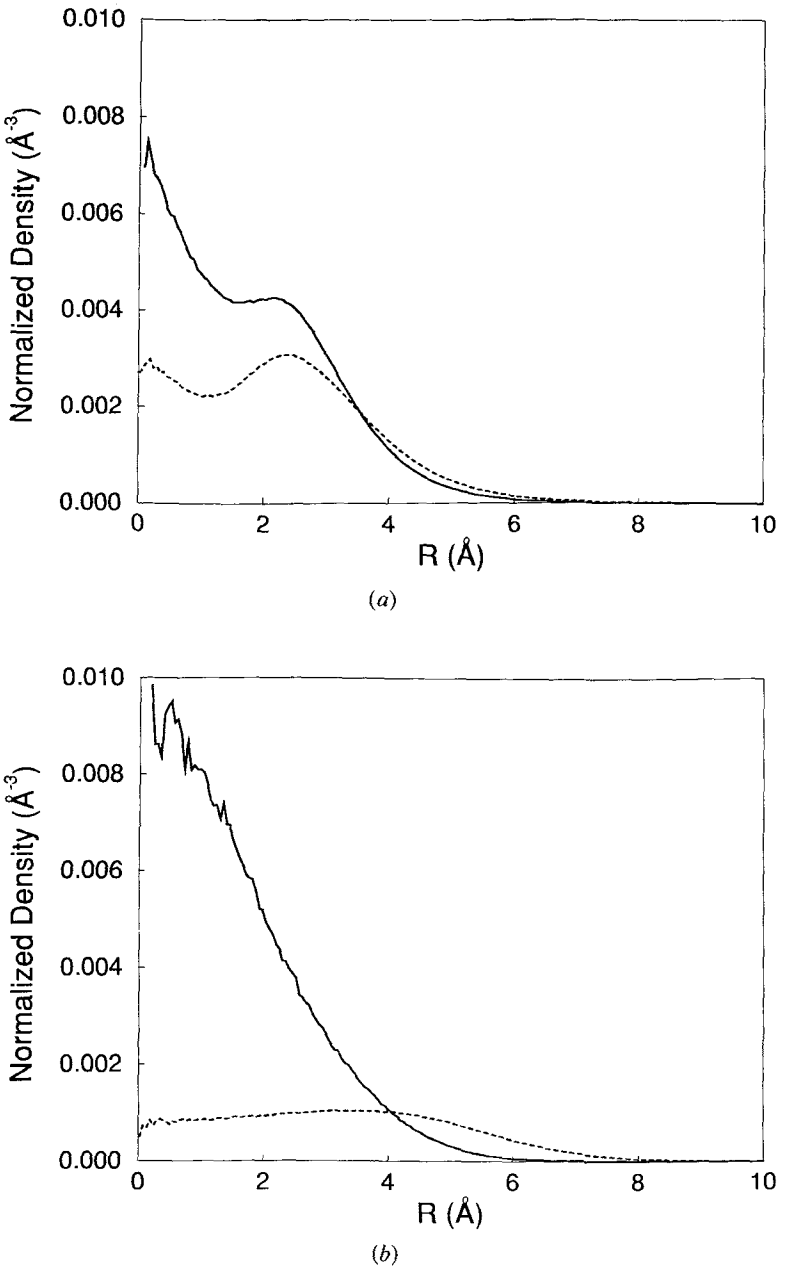

Figure 5. Single-particle radial density profiles for ground state D_2He_N clusters: (*a*) $N=2$; (*b*) $N=13$. The broken and solid curves refer to helium and to D_2, respectively, and are normalized to one particle per cluster in each case; VCM results. (From Barnett *et al.* 1993.)

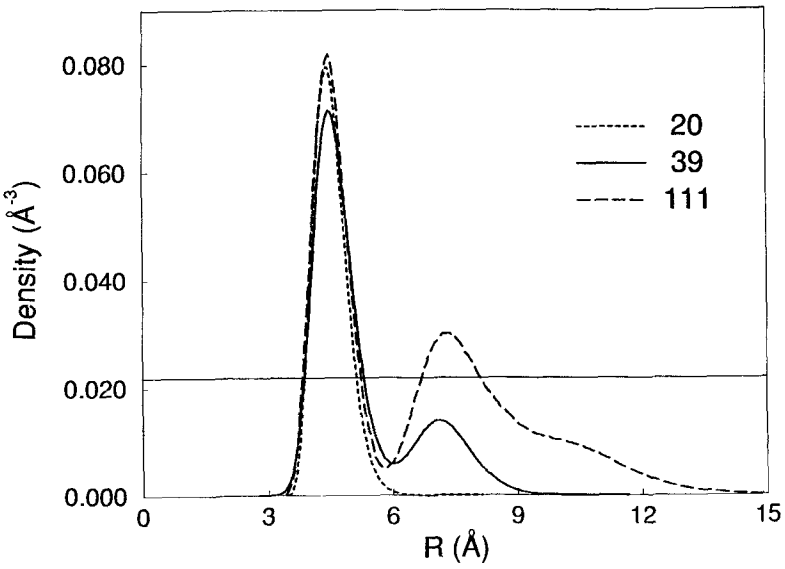

Figure 6. Single-particle radial He density profiles for ground-state SF_6He_N; $N=20$, 39 and 111; anisotropic SF_6–He interaction incorporated; second-order estimates from DMC calculations. (From Barnett and Whaley 1993b.)

these rates increase and appear to become statistical for large enough N. Dalfovo (1989) has used the density-functional approach (see below) to analyse the surface states of ^{3}He on clusters of ^4He_N and has compared the results with those of a variational calculation based on the trial wavefunction

$$\psi(\mathbf{r}_1 \ldots \mathbf{r}_N)=f(\mathbf{r}_1)\psi_0(\mathbf{r}_1 \ldots \mathbf{r}_N), \tag{3.17}$$

where $\mathbf{r}_1$ is the coordinate of the ^{3}He atom, and $\mathbf{r}_i$, $i=2$–N, are the coordinates of the ^{4}He atoms. Good agreement is obtained between the two approaches, both of which predict an effective potential with a well in the surface region giving rise to stable surface-bound ground states with energies scaling with the surface curvature, that is $N^{-1/3}$. This is consistent with the occurrence of surface states on bulk ^{4}He (Andreev states) and follows from the balance of excess kinetic energy of one ^{3}He in the bulk, and the binding energy of He–He. Higher-energy states are found to enter the cluster, that is at energies exceeding the central value of the effective potential.

3.4. *Mean-field and density-functional studies*

This approach, first applied to helium clusters by Stringari and Treiner (1987), has the advantage of involving much simpler calculations than the QMC method. Mean-field theories can also be extended to provide approximations for excited states and dynamical effects (§ 4). Stringari and Treiner (1987) use a phenomenological non-local Skyrme interaction to derive Hartree–Fock equations for single-particle wavefunctions for both ^4He_N and ^3He_N. The resulting ground-state properties for the Bose clusters (^4He_N) are in good agreement with the prior QMC calculations. For the Fermi clusters (^3He_N) the binding threshold was found to be $N=30$, and marked shell effects

were found. The single-particle energy levels were found to fall into sets consistent with the filling of energy shells for a harmonic oscillator potential

$$H=\sum\left(\frac{p_i^2}{2m^*}+\tfrac{1}{2}m^*\omega_0^2 r_i\right), \tag{3.18}$$

where ω_0 constitutes a single-particle energy gap and m^* is an effective mass. Even though the self-consistent potential energy well is finite, the degeneracy of the energy level structure was found to fit the harmonic oscillator model better than that of a square well. The resulting magic numbers of enhanced stability were predicted as $N=40, 70, 112, 168, 240, \ldots$. Despite clear indications of such shell structure in the energetics, no oscillations were seen in the ground-state densities however. The density-functional approach results in very smooth monotonic profiles for both isotopes, unlike the prior VMC calculations of Pandharipande *et al.* (1986) which had some density oscillations for the Fermi systems. The lack of density oscillations in the mean-field results was attributed to the high effective mass for ^{3}He ($m^*=2{\cdot}8m_3$), but clearly this is a structural detail lost in the density-functional approach. Stringari and Treiner (1987) also make an interesting analysis of the relative compression $\delta\rho/\rho_0=(\rho_c-\rho_0)/\rho_0$, where ρ_c is the central density and ρ_0 the bulk density, showing that, for both types of cluster, deviations occur from the behaviour expected for saturated systems. In particular, for $N<200$, the clusters appear pachidermous, that is less compressed than the idealized saturated systems while, for larger N, the clusters become leptodermous, that is more compressed, and there is a monotonic decrease in $\delta\rho/\rho_0$ below zero as N increases further.

4. Excited states

Here we summarize theoretical investigations of excited states of quantum clusters. We shall deal only with isolated excited states, leaving the question of thermodynamic averages over these states to § 5. Most work has focused on the study of collective excitations, which can be divided into compressional, surface and rotational collective modes. Single-particle excitations out of the ground state have been analysed within both the mean-field (Stringari and Treiner 1987) and variational (Lewart *et al.* 1988) approaches but can be expected to be less significant than the collective modes. Because of the liquid nature of helium clusters, valuable qualitative insight into the collective modes has been provided by the liquid-drop model (LDM) common in nuclear physics, which is based on classical hydrodynamics. We therefore first summarize the application of this classical model to He_N and its predictions in § 4.1. We describe the quantum-mechanical generalization of the liquid-drop model (QLDM) in § 4.2. Variational approaches to the excited states are then discussed in § 4.3, and § 4.4 contains a summary of estimates made within the random-phase approximation.

4.1. *A classical liquid-drop model*

In this model the cluster ground or equilibrium state is assumed to be spherical, to have a uniform interior density and to be terminated by a sharp surface at R_0 (Bohr and Mottelson 1975). This is a reasonable approximation for large helium clusters (figure 2), although the surface always has an intrinsic diffuseness of about 7 Å. The collective excitations are then obtained by making quadratic expansions of the density in the

appropriate coordinates. For surface vibrations the coordinates are obtained from an expansion of the surface shape in the spherical harmonics:

$$R(\theta,\phi)=R_0\left(1+\sum_{lm}\alpha_{lm}Y^*_{lm}(\theta,\phi)\right), \tag{4.1}$$

while for compressional modes the collective coordinate is the local density fluctuation

$$\delta\rho(\mathbf{r})=\rho_0\, j_l(k_{nl}r)Y^*_{lm}(\theta,\phi)\alpha_{lmn}. \tag{4.2}$$

These normal coordinates oscillate harmonically in time, with frequencies given by

$$\omega_l=\left(\frac{4\pi}{3}l(l-1)(l+2)\frac{\zeta}{Nm_{\mathrm{He}}}\right)^{1/2} \tag{4.3}$$

and

$$\omega_{ln}=k_{nl}u_c=k_{nl}\left(\frac{1}{K\rho_0 m_{\mathrm{He}}}\right)^{1/2} \tag{4.4}$$

for surface and compression modes of angular symmetry l, respectively. ζ is the surface tension and K the bulk compressibility. Compressional modes have additional radial nodal structure, indexed by n. Values of k_{nl} are given by the boundary condition $\delta\rho(R_0)=0$, for example $k_{10}=\pi/R_0$. The restoring force for surface modes is provided by the surface tension ζ, which opposes surface deformation, and for compressional modes by the bulk compressibility K. Generally the surface modes lie lower in energy than compressional modes, as illustrated by the ratio of lowest surface mode, the quadrupole $l=2$, to the lowest compressional mode, the breathing mode with $l=0$ and $n=1$:

$$\frac{\omega_2}{\omega_{10}}=\left(\frac{4}{3}\right)^{1/2}\frac{2^{1/2}}{\pi N^{1/6}}\left(\frac{b_{\mathrm{surf}}}{b_{\mathrm{comp}}}\right)^{1/2}, \tag{4.5}$$

where $b_{\mathrm{surf}}=4\pi r_0^2\zeta$ and $b_{\mathrm{comp}}=(K\rho_0)^{-1}=u_c^2 m_{\mathrm{He}}$. (Note that $R_0=r_0N^{1/3}$.) For helium, the bulk values of the speed of sound $u_c=238\ \mathrm{ms}^{-1}$ and surface tension $\zeta=0{\cdot}274K\ \text{Å}^{-2}$, yield 0·68 for the ratio $b_{\mathrm{surf}}/b_{\mathrm{comp}}$, resulting in 0·10 for the ratio of lowest surface to lowest compression mode at $N=720$ particles. Despite the very low compressibility of helium, this ratio is similar to the corresponding values for very different materials such as water (0·08) and nuclear matter (0·13), because the surface tension is also very low for helium.

As demonstrated in §4.2, the quantum analogue of the LDM gives significantly lower excitation energies. However, the classical LDM predictions provide useful qualitative understanding of the collective modes and, being analytic, have also lent themselves to a number of quantum-statistical treatments of finite-temperature properties. These will be discussed in §5.1.

4.2. *Quantum liquid-drop model*

The QLDM was developed by Krishna and Whaley (1990a, b) to describe compressional excitations of liquid-helium clusters. Instead of deriving a wave equation with boundary conditions imposed by the sharp liquid-drop surface, as is done in the classical model, the quantum approach starts from the Bose quantum fluid Hamiltonian description of the cluster and expands the quantum density functional about the ground-state density (Krishna and Whaley 1990b):

$$H[\rho]=U[\rho_0]+\tfrac{1}{2}\rho_0 m_{\mathrm{He}}\int|\mathbf{v}|^2(\mathbf{r})\,\mathrm{d}^3r+\tfrac{1}{2}\int\phi(\mathbf{r}_1,\mathbf{r}_2)\delta\rho(\mathbf{r}_1)\delta\rho(\mathbf{r}_2)\,\mathrm{d}^3r_1\,\mathrm{d}^3r_2. \tag{4.6}$$

Applying the boundary condition

$$\delta\rho(r=R_0)=0, \tag{4.7}$$

expanding in spherical harmonics and applying hydrodynamic continuity lead to the harmonic expansion

$$H[\rho]=U[\rho_0]+\sum_{lmn}\left(\frac{1}{2}\frac{|\dot{\rho}_{lmn}|^2}{\rho_0 k_{ln}^2}m_{\mathrm{He}}v_{ln}+\tfrac{1}{2}\phi_{0n}|\rho_{lmn}|^2 v_{ln}^2\right), \tag{4.8}$$

where $\rho_{lmn}=\rho_0\alpha_{lmn}$ (see equation (4.2)), v_{ln} is a normalization constant and ϕ_{0n} are the expansion coefficients of the general non-local compressibility $\phi(\mathbf{r}_1,\mathbf{r}_2)$. Employing the virial theorem to eliminate ϕ_{0n} then yields the dispersion relation

$$\varepsilon_{lmn}=\frac{\hbar^2 k_{ln}^2}{2m_{\mathrm{He}}S_{lm}(k_{ln})v_{ln}}, \tag{4.9}$$

where

$$S_{lm}(k_{ln})=\frac{\langle|\rho_{lmn}|^2\rangle}{\rho_0}$$
$$=\frac{1}{\rho_0 v_{ln}^2}\int\int \mathrm{d}\mathbf{r}_1\,\mathrm{d}\mathbf{r}_2 j_l(k_{ln}r_1)j_l(k_{ln}r_2)Y_{lm}^*(\hat{\mathbf{r}}_1)Y_{lm}(\hat{\mathbf{r}}_2)\langle\delta\rho(\mathbf{r}_1)\delta\rho(\mathbf{r}_2)\rangle. \tag{4.10}$$

Equation (4.9) is the spherical cluster analogue of the Bijl-Feynman result for the longitudinal excitations of bulk helium (Feynman 1954):

$$\varepsilon_k=\frac{\hbar^2 k^2}{2m_{\mathrm{He}}S(k)}, \tag{4.11}$$

where $S(k)$ is the bulk structure function. Note that the definitions of k differ for the cluster and bulk equations.

Figure 7 shows the excitation energies for $l=0$, 1 and $m=0$, for He_N with $N=20$, 70 and 240 (Krishna and Whaley 1990c). The Bijl–Feynman spectrum is shown as a solid curve for comparison. The latter shows the characteristic linear phonon dispersion at small k, and the minimum at around $k=2$ Å^{-1}, which is known as the roton minimum. For a given size N, the discrete cluster energy levels lie on smooth dispersion curves, with the $l=0$ and $l=1$ levels alternating. The most striking feature is the evolution of the dispersion curves with N to approach the bulk longitudinal spectrum. For $N=20$, the spectrum is monotonically increasing with perhaps a hint of a shoulder at $k=1$ Å^{-1}, but no structure in the roton region. For $N=70$ there is now a shoulder at $k\approx 1{\cdot}3$ Å^{-1}, and an incipient minimum at $k\approx 1{\cdot}8$ Å^{-1}. The largest cluster $N=240$ now shows a pronounced roton minimum, at a smaller k than in the bulk, and also shows an approximately linear region at small k with slope comparable with that in the bulk. The interpretation of the size dependence relies on the significance of the roton structure in the bulk spectrum. The Bijl–Feynman result is a faithful representation of the features of the experimental dispersion curve measured from neutron scattering, although the theoretical energies are too high. In particular, the excitations in the roton region are observed to broaden and disappear above the superfluid transition temperature T_λ (Tilley and Tilley 1986). While the atomic dynamics in the roton collective excitations are not well understood in the bulk, they are nevertheless regarded as a signature of superfluidity because they are found only in the superfluid state. Thus the finite cluster spectra lead to the conclusion that clusters of $N>70$ are in a superfluid ground state,

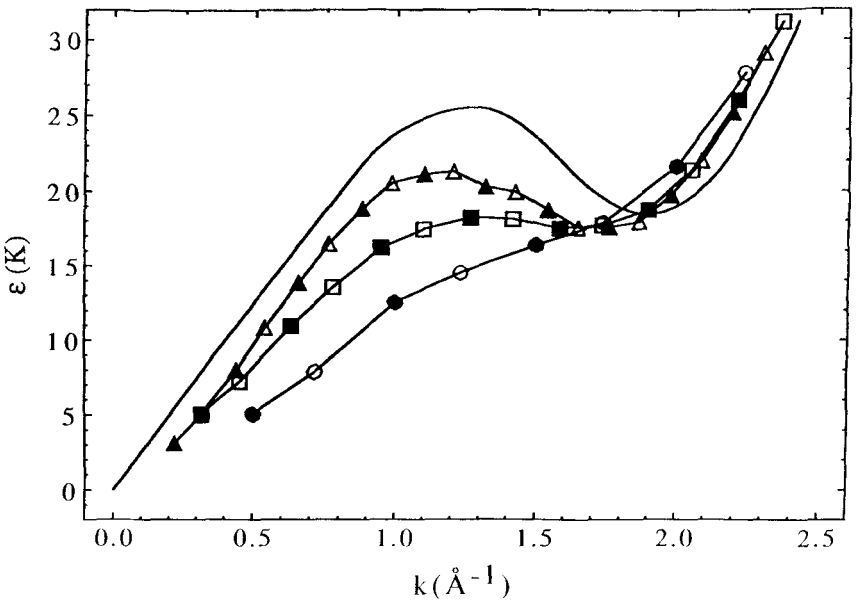

Figure 7. QLDM cluster excitation spectra for $l=0$ (●, ■, ▲) and $l=1$ (○, □, △): (●), (○), $N=20$; (■), (□), $N=70$; (▲), (△), $N=240$; ——, the Bijl–Feynman spectrum for bulk ^{4}He. (From Krishna and Whaley 1990c.)

while the smaller cluster, $N=20$, is not superfluid. This predicted onset of fluidity at $N \approx 70$ from the elementary excitation spectrum is consistent with the conclusions of the finite-temperature path integral studies which will be discussed in § 5.

Two important approximations are made in the QLDM, which should be mentioned. The first is the sharp liquid surface assumption, and the second is a diagonal approximation to the potential energy (Krishna and Whaley 1990b). Quantitative analysis shows that the former is quite well justified for helium clusters larger than $N=20$, as might be expected from the profiles in figure 1. The second approximation affects the interpretation of the dispersion curves shown above. The QLDM result for the compressional excitations implies both radial (n) and angular (l, m) symmetry, both of which are essential for the derivation of the dispersion relation equation (4.9) between the energy and the spherical wavevector k_{ln}. However, this dispersion relation is an approximation for a finite system since only the angular symmetry is a true symmetry of the system. The presence of radial nodal structure results from the neglect of off-diagonal coupling which arises from the long-range nature of the non-local compressibility $\phi(\mathbf{r}_1, \mathbf{r}_2)$. This approximation, essential to the harmonic expansion analysis, can be avoided in the excitation operator approach described in § 4.3, in which case it leads to a spectrum of energy levels from which evidence of the roton structure has to be inferred indirectly from, for example the density of states.

4.3. *Variational approaches*

Variational calculations based on an excitation operator approach to excited states have greater generality than the QLDM and are more flexible. In the excitation operator approach the excited state is written as

$$\psi_e = F(\mathbf{R})\psi_0, \tag{4.12}$$

where ψ_0 is the ground state and $F(\mathbf{R})$ is some excitation operator to be determined. This forms the starting point of a variety of theoretical treatments of excited states, for example for the coupled-cluster expansion in quantum chemistry (Bartlett 1989), and for the Bijl–Feynman treatment of bulk helium compressional excitations (Bijl 1940, Feynman 1954, Feynman and Cohen 1957). When the ground state ψ_0 is known exactly, one can obtain a variational bound on the first excited state:

$$\varepsilon = \frac{\langle \psi_e | H - E_0 | \psi_e \rangle}{\langle \psi_e | \psi_e \rangle} \tag{4.13}$$

but, if the ground state is itself variational, no variational bound on ε exists.

The situation is different when the excited states have different symmetries from the ground state. Now excited states with angular symmetry (l, m) can be obtained variationally from excited-state *ansatzes* derived either from the $l=0$ ground state or from other $l=0$ functions:

$$\psi_e^{(lm)} = F^{(lm)}(\mathbf{R})\psi_0^{(00)}. \tag{4.14}$$

Here $\psi_0^{(00)}$ is either the ground state or a ground-state-like function. This has recently been exploited to obtain excited surface vibrational states with $l=2$ (Chin and Krotscheck 1992), and for rotationally excited and deformed states of the cluster as a whole (McMahon *et al.* 1993).

We discuss first the compressional excitation energies for $l=0$ which have been obtained from action of an excitation operator on variational ground states. Krishna and Whaley (1990d) employed a collective operator of the form

$$F_n = \sum_{i=1}^{N} \exp(-\alpha_{0n} r_i^2) j_0(k_{0n} r_i) Y_{00}(\hat{\mathbf{r}}_i) \tag{4.15}$$

where both α_{0n} and k_{0n} are treated as variational parameters. For k_{ln} held constant at the sharp liquid surface value determined by

$$j_l(k_{ln} R_0) = 0, \tag{4.16}$$

$$F'_n = \sum_{i=1}^{N} j_l(k_{ln}) Y_{lm}(\hat{\mathbf{r}}_i) - \frac{1}{N} \left\langle \sum_i j_l(k_{ln} r) Y_{lm}(\hat{\mathbf{r}}_i) \right\rangle \tag{4.17}$$

was shown to yield the QLDM result. The variational approach can also be combined with a Gram–Schmidt orthogonalization procedure to obtain successively orthogonal excited states. Krishna and Whaley (1990d) applied this to the first four compressional excitations of $l=0$, beyond which it becomes exceedingly cumbersome. The resulting energies are shown in table 3, together with the QLDM and classical LDM estimates of these. It is clear that the Krishna–Whaley orthogonalized variational excitation operator energies lie consistently below the liquid-drop estimates, although the difference between non-variational results and the QLDM (Krishna and Whaley 1990b) does decrease with increasing size N. In fact the LDM predicts that all collective monopole modes are metastable with respect to single-particle dissociation, that is

$$\hbar\omega + \mu > 0, \tag{4.18}$$

where μ is the chemical potential (equation 3.8) (Chin and Krotscheck 1992). In contrast, the orthogonalized variational energies are bound for all N, while the QLDM energies only become bound for $N = 240$, consistent with the improved validity of the sharp liquid surface approximation for larger N.

Table 3. Compressional excitations for He_N clusters: KW, variational results of Krishna and Whaley (1990d); QLDM, quantum liquid-drop model (Krishna and Whaley 1990b); LDM, classical liquid-drop model, equations (4.3) and (4.4) (Krishna and Whaley 1990d); CK, variational results of Chin and Krostcheck (1992), obtained with the HFDHE potential (Aziz *et al.* 1979). KW and QLDM employ the HFD–B(HE) potential (Aziz *et al.* 1987).

			Compressional excitation (K)				
l	n	Method	$N=20$	$N=40$	$N=70$	$N=112$	$N=240$
0	1	KW	2·67		3·9		2·87
0	1	CK	2·80	3·68	3·97	4·21	
0	1	QLDM	6·05		4·93		3·00
0	1	LDM	9·48	7·52	6·24	5·34	4·14
0	2	KW	3·9		5·5		4·70
0	2	QLDM	13·23		11·81		7·76
0	2	LDM	18·96	15·04	12·48	10·67	8·28
0	3	KW	5·6		7·6		6·16
0	3	QLDM	15·56		17·07		13·59
0	3	LDM	28·43	22·57	18·73	16·01	12·42
0	4	KW	8·1		13·7		7·80
0	4	QLDM	19·95		18·73		18·52
0	4	LDM	37·91	30·09	24·97	21·35	16·56
2	1	CK	1·71	1·22	1·03	1·20	
2	1	LDM	2·32	1·64	1·24	0·98	

Chin and Krotscheck (1990, 1992) have studied the lowest excited states derived from DMC second-order ground-state densities. They employ the general formula

$$E-E_0=\frac{\langle\psi_0|F[H,F]|\psi_0\rangle}{\langle\psi|F^2|\psi_0\rangle}, \tag{4.19}$$

with F given as a sum of one-particle operators:

$$F=\sum_{i=1}^{N} f_i-\langle f_i\rangle. \tag{4.20}$$

This is used to obtain the eigenvalue equation for excited states,

$$H_1 u(\mathbf{r})=\hbar\omega\int d\mathbf{r}'\, S(\mathbf{r},\mathbf{r}')u(\mathbf{r}'), \tag{4.21}$$

where

$$u(\mathbf{r})=[\rho_1(\mathbf{r})]^{1/2}f(\mathbf{r}), \tag{4.22}$$

$S(\mathbf{r},\mathbf{r}')$ is the static structure function, $\rho_1(\mathbf{r})$ is the single-particle density and H_1 is a non-local kinetic energy operator (Chin and Krotscheck 1990). The one- and two-particle densities required to evaluate $S(\mathbf{r},\mathbf{r}')$ are estimated from the second-order approximation, equation (3.15). Equation (4.21) is then solved for the excited states l resulting from a partial wave expansion. Results for the monopole ($l=0$) and dipole ($l=2$) modes are also listed in table 3 and show that the $l=0$ excitation is very close to the Krishna–Whaley variational result. The dipole excitation lies somewhat lower in energy, as

expected for surface vibrations from the LDM analysis (§ 4.1). The surface nature of this mode is also evident from the transition density $\rho_{tr}(\mathbf{r}) = \langle \psi_0 | \hat{\rho} | \psi_e \rangle$ which shows structure in the surface region (Chin and Krotscheck 1990).

The construction of excited states with non-zero l poses interesting interpretation problems, because these can occur in all three types of excitation, namely compressional, surface and overall rotation. Despite the use of a variational technique, the nature of the $l \neq 0$ mode obtained will depend strongly upon the restrictions placed by the choice of excitation operator $F(\mathbf{R})$. Thus, while the surface excitations were obtained by Chin and Krotscheck (1990, 1992) with a sum of single-particle operators depending on the distance from the centre of mass (equation 4.20), it is possible to obtain quite different excitations with lower variational energies by taking F in another approach: a sum of two- or higher-particle functions. This has recently been exploited to study rotationally excited states for both helium and molecular hydrogen clusters (McMahon *et al.* 1993).

The approach of McMahon *et al.* (1993) differs from the original excitation operator approach of Feynman in that the excitation function $F^{(lm)} = \chi_{lm}$ is of fixed form while the remaining factor, $\psi_0' = \psi_0^{(00)}$, need not describe the ground state. Instead, ψ_0' is optimized to obtain the variationally optimal energy for the lowest state of angular symmetry lm:

$$\psi_{lm} = \chi_{lm} \psi_0'. \tag{4.23}$$

ψ_0' is taken to have the same parametric form as the true ground state ψ_0. The role of χ_{lm} is therefore to impose the lm symmetry for a given type of excitation, in this case of overall rotation. Applications have been made for states with $m = l$, noting that, in the absence of a magnetic field, all $2l+1m$ states are degenerate. A simple function for rotational excitations is given by the symmetrized sum of two-particle diatomic functions:

$$\chi_{ll} = \sum_{i<j} \phi_{ll}(r_{ij}), \tag{4.24}$$

$$\phi_{ll}(r_{ij}) = \left(\frac{x_{ij} + i y_{ij}}{r_{ij}} \right)^l, \tag{4.25}$$

which is an eigenvector of total angular momentum L, that is

$$\begin{aligned} \hat{L}^2 \chi_{ll} &= l(l+1)\hbar^2 \chi_{ll}, \\ \hat{L}_z \chi_{ll} &= l_z \hbar \chi_{ll}. \end{aligned} \tag{4.26}$$

Note that $\phi_{ll}(r_{ij})$ is simply proportional to the spherical harmonic $Y_{ll}(\theta_{ij}, \phi_{ij})$. Thus the excited state

$$\psi_{ll} = \chi_{ll} \psi_0 \tag{4.27}$$

has a clear physical interpretation of a permutation symmetrized sum of overall rotation due to relative angular momentum introduced by pairs of particles. This form is restricted to even L. An improved variational ansatz is provided by the function

$$\begin{aligned} \chi_{ll} &= \sum_i (X_i + i Y_i)^l, \\ X_i &= \sum_{j \neq i} x_{ij}, \quad Y_i = \sum_{j \neq i} y_{ij}, \end{aligned} \tag{4.28}$$

in which the collective coordinates X and Y bear a formal similarity to the two-particle coordinates x and y in equation (4.25). Since X_i is proportional to $x_i - X_{lm}$ likewise for Y_i), equations (4.28) may be interpreted as a permutation symmetrized sum of relative angular momentum of all particles about the cluster centre of mass. The function can be viewed as derived from the one-particle function $(x_i + iy_i)^l$ by making it translationally invariant and then symmetrizing it. One can verify that equation (4.28) possesses the eigenvalues given in equation (4.26) and is therefore a valid trial wavefunction. Although these are now complex wavefunctions, Monte Carlo evaluation of the ground-state energy is no more complicated that for real functions. In practice the energy, and other quantities of interest, can be obtained from either the real or imaginary parts of the wavefunction.

Figure 8 shows VMC contour plots for He_7 of the density distribution function $\rho(z, r)$, where z is measured along the axis of rotational quantization and r is the two-dimensional radial coordinate in the x–y plane. The monotonically decreasing spherical density seen for $l=0$ is increasingly distorted as l increases, first to oblate shapes still with diffuse, monotonically decreasing density, and later to toroidal shapes as a depression near $r=0$ sets in. This kind of distortion with increasing rotational excitation is qualitatively similar to the distortions of classical liquid droplets studied by Chandrasekhar (1965), summarized in figure 9. One significant difference, however, is the density expansion. Detailed analysis shows that for the diffuse surface quantum droplet this occurs both in the x–y plane and to a lesser extent in the z direction. The classical sharp-surface droplets show an expansion only in the x–y plane and show a marked compression in the z direction (figure 9). The smooth shape of the surface region showing only the oblate distortion and not an average spherical shape confirms that these are indeed overall rotational states of the cluster, as opposed to the localized surface vibrations studied by Chin and Krotscheck (1990, 1992).

Figure 10 shows the corresponding contour plots for $(H_2)_7$. Here a similar general trend of expansion and oblate distortion with increasing l is seen, but there are important quantitative differences imposed by the greater degree of rigidity of this system. While there is also expansion in the x–y plane, it is not so pronounced and, as in classical systems, there is now a compression rather than an expansion in the z direction. The ridge of maximum density for $l=0$, absent in He_7, is significantly distorted in the larger l states, with a symmetry breaking to form a high-density region located on or close to the z axis, while the lower part of the ridge near the x–y plane is essentially dispersed radially to form a very diffuse low-density extension in and about the x–y plane. This is consistent with a large centrifugal distortion of a ring of atoms in the equatorial plane, and a much smaller centrifugal distortion of a smaller number of atoms located close to the z axis away from the x–y plane. It therefore supports the conjecture made for the $l=0$ structure, that there is a significant contribution of pentagonal bipyramidal-like structures to $(H_2)_7$.

Analysis of the VMC energetics reveals that all these rotationally excited states for He_7 are metastable with respect to dissociation to $He_6 + He$, while, for $(H_2)_7$, states with $l>5$ become metastable. Similar conclusions are reached with fixed-node DMC calculations using these variational functions as trial functions. The DMC second-order density contours show the same kind of distortions as the VMC contours in figures 8 and 10, with somewhat larger distortions for He_7 at a given value of l (McMahon *et al.* 1993).

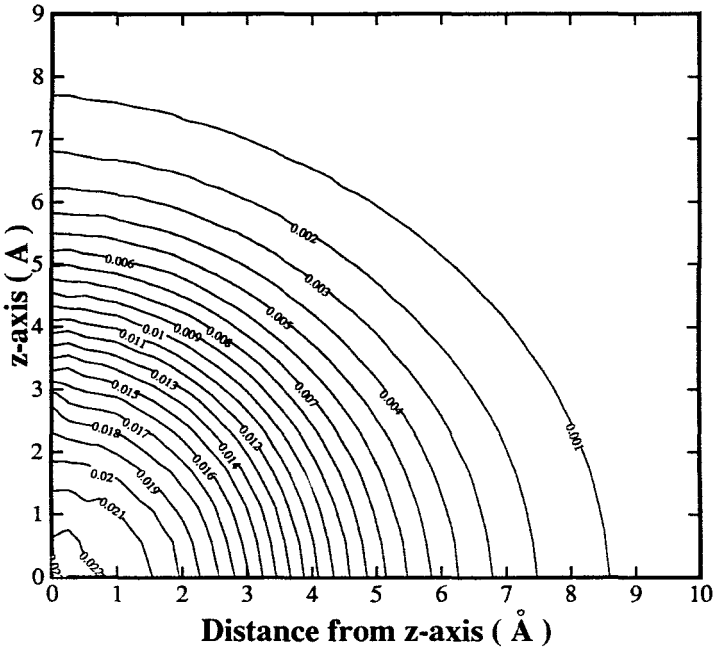

(*a*)

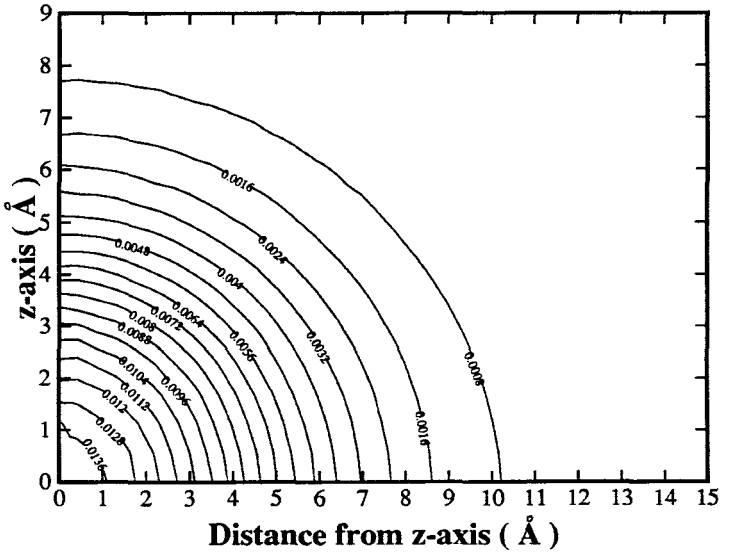

(*b*)

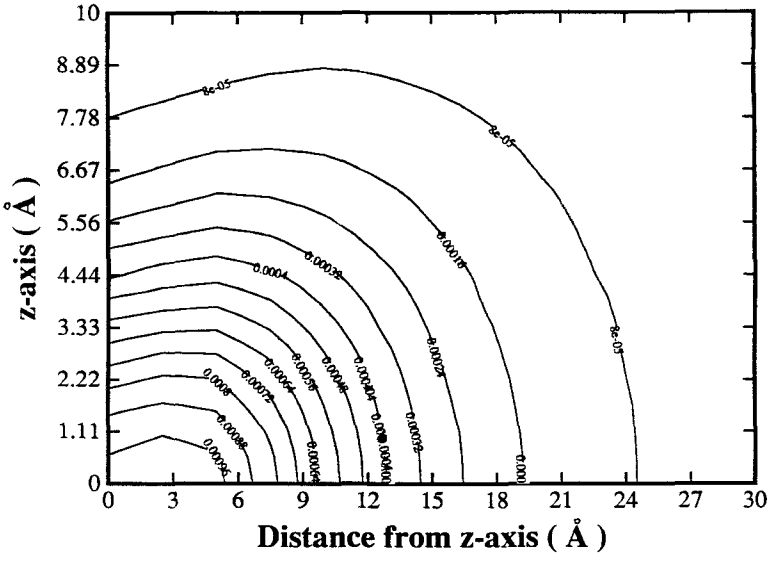

(*c*)

Figure 8. Contour plots for the density distribution $\rho(z, r)$ for He_7 rotationally excited states: (*a*) $l=2$; (*b*) $l=4$; (*c*) $l=6$. ρ is the two-dimensional radial coordinate in the x–y plane perpendicular to the z axis of quantization. (From McMahon *et al.* 1993.)

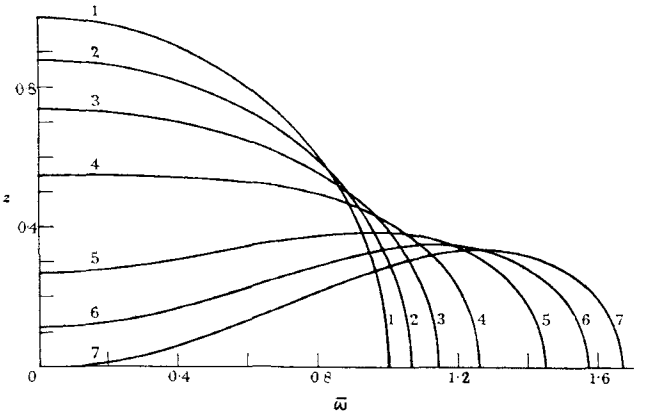

Figure 9. Shape distortions of a rotating classical liquid drop as a function of increasing rotation velocity from curves 1 to 7. $\bar{\omega}$ denotes the two-dimensional radial coordinate in the x–y plane perpendicular to the z axis of rotation. (From Chandraskhar 1965.)

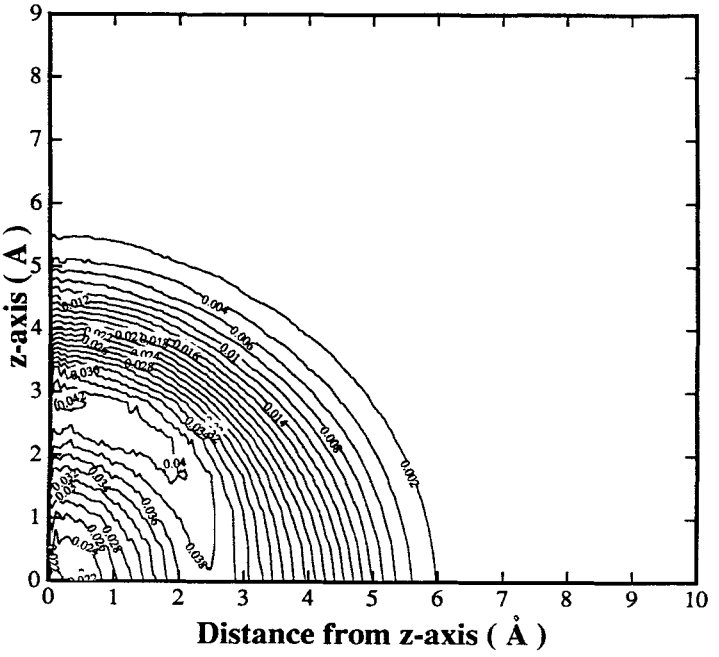

(*a*)

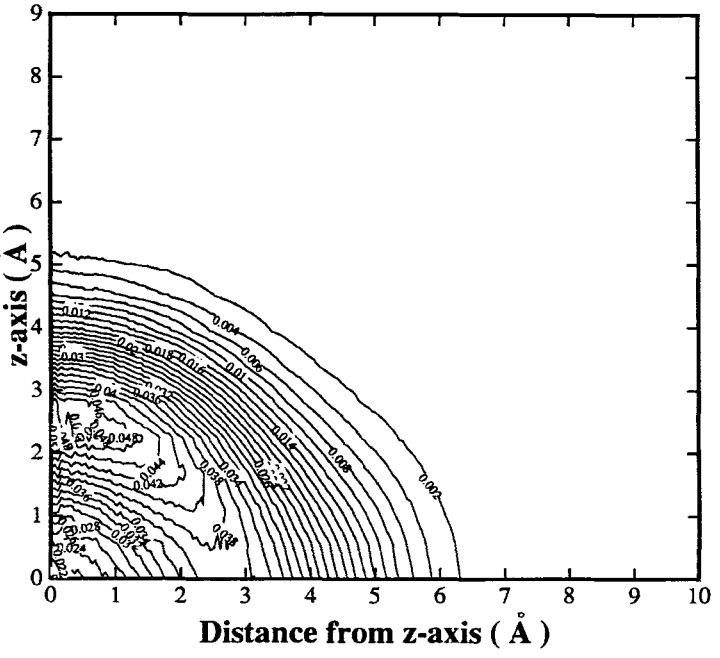

(*b*)

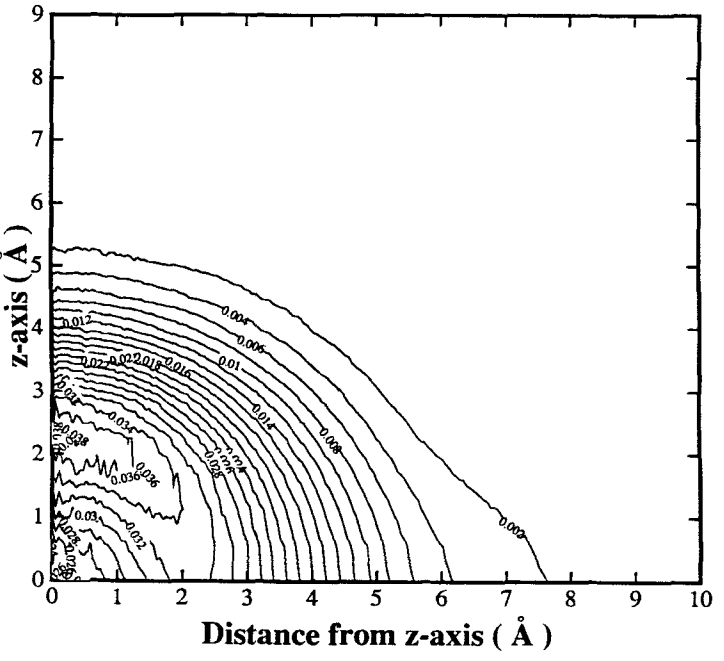

(*c*)

Figure 10. Contour plots for the density distribution $\rho(z, r)$ for $(H_2)_7$ rotationally excited states: (*a*) $l=2$; (*b*) $l=5$; (*c*) $l=7$. ρ is the two-dimensional radial coordinate in the x–y plane perpendicular to the z axis of quantization. (From McMahon *et al.* 1993.)

4.4. *Low-lying excitations from the random-phase approximation*

Casas and Stringari (1990) have extended the mean-field density-functional approach to a self-consistent calculation of collective excitations within the random-phase approximation (RPA). The RPA provides a good description of long-range correlation and has been used successfully to treat phonons and ripplons in bulk ^{4}He (Krotscheck *et al.* 1987), as well as collective phenomena (giant resonances) in atomic nuclei (Bertsch and Tsai 1975, Liu and van Giai 1976). They use the Green function formulation of RPA (Bertsch and Tsai 1975) in which the particle–hole Green function is given by solution of the integral equation

$$G_{\mathrm{RPA}}(\mathbf{r}_1, \mathbf{r}_2, \omega) = G_0(\mathbf{r}_1, \mathbf{r}_2, \omega) + \int G_0(\mathbf{r}_1, \mathbf{r}_3, \omega) V_{\mathrm{ph}}(\mathbf{r}_3, \mathbf{r}_4) G_{\mathrm{RPA}}(\mathbf{r}_4, \mathbf{r}_1, \omega)\, \mathrm{d}\mathbf{r}_3\, \mathrm{d}\mathbf{r}_4, \tag{4.29}$$

where V_{ph} is the residual particle–hole interaction given by

$$V_{\mathrm{ph}} = \frac{\delta^2 E_{\mathrm{c}}}{\delta\rho(\mathbf{r}_1)\delta\rho(\mathbf{r}_2)}, \tag{4.30}$$

and G_0 is the Hartree–Fock Green function

$$G_0(\mathbf{r}_1, \mathbf{r}_2, \omega) = \sum_n \frac{\phi_0^*(\mathbf{r}_1)\phi_0(\mathbf{r}_2)\phi_n^*(\mathbf{r}_2)\phi_n(\mathbf{r}_1)}{\omega - \omega_{n0} + \mathrm{i}\varepsilon} - \frac{\phi_0^*(\mathbf{r}_2)\phi_0(\mathbf{r}_1)\phi_n^*(\mathbf{r}_1)\phi_n(\mathbf{r}_2)}{\omega + \omega_{n0} + \mathrm{i}\varepsilon}. \tag{4.31}$$

Self-consistency derives from taking the energy function $E_{\mathrm{c}}(\rho)$ to be the same interaction energy functional used for the ground-state Hartree–Fock solution

(Stringari and Treiner 1987). The particle–hole Green function is also a density–density correlation function (Doniach and Sondheimer 1974, Bertsch and Tsai 1975) and its poles yield the excited vibrational states. In practice, equation (4.32) is solved in coordinate space as a separate matrix equation for each lm after making a multipole decomposition in spherical harmonics (Casas and Stringari 1990). The response function

$$\chi_F(\omega(= \int f^*(\mathbf{r}_1) G_{\mathrm{RPA}}(\mathbf{r}_1, \mathbf{r}_2, \omega) f(\mathbf{r}_2)\, \mathrm{d}\mathbf{r}_1\, \mathrm{d}\mathbf{r}_2 \tag{4.32}$$

is then evaluated by quadrature for a given excitation operator

$$F = \sum_i f(\mathbf{r}_i). \tag{4.33}$$

The excitation energies are then given by the poles of $\chi_F(\omega)$. The relationship between this density-functional–RPA theory and the variational approach of the previous section has been discussed by Chin and Krotschek (1992).

This RPA analysis was used to evaluate the lowest vibrational excitations of ^4He_N clusters as a function of size. Figure 11 summarizes the size dependence of the $L=0$ monopole compression mode and of the $L=2$ quadrupole surface modes. Both modes show a clear convergence to the classical LDM limits by $N \approx 728$ and indicate that deviations from the LDM are important up to $N \approx 500$ for compression and up to $N \approx 100$ for surface modes. Like the variational results, the RPA excitation energies also lie consistently below the LDM. However, they do lie significantly above the zeroth-order Hartree–Fock estimates, showing the increasing importance of incorporating the long-range density correlations in the excited state as N increases, whether this is done by RPA or by appropriate choice of variational wavefunction. A detailed quantitative comparison of the RPA and variational results for the lowest monopole and quadrupole excitations has been given by Chin and Krotscheck (1992).

The transition densities between ground state $|0\rangle$ and excited state $|n\rangle$ given by

$$\rho_{\mathrm{tr}}(\mathbf{r}) = \langle 0| \sum_i \delta(\mathbf{r} - \mathbf{r}_i) |n\rangle \tag{4.34}$$

can also be obtained from the Green function, via the relation

$$\rho_{\mathrm{tr}}(\mathbf{r}) = \int G_{\mathrm{RPA}}(\mathbf{r}, \mathbf{r}') f(\mathbf{r}')\, \mathrm{d}\mathbf{r}'. \tag{4.35}$$

The RPA results for these show the characteristic behaviour expected of vibrational modes. Thus the monopole density has a single maximum in the cluster interior and no nodes, while the quadrupole surface density has oscillations about a single node in the surface region.

5. Finite-temperature studies

The previous sections have dealt exclusively with the properties of isolated eigenstates and have been primarily concerned with ground-state $T=0$ behaviour. Although the temperature of the gas-phase He_N and $(H_2)_N$ clusters is not well characterized, it is expected on experimental grounds to be about 0·4 K for He_N (Bucheneau *et al.* 1990) and about 6 K for $(H_2)_N$ (Knuth *et al.* 1990, Goyal *et al.* 1992b). Since this is of the same order of magnitude as the rotational and vibrational excitations for He_N, it is important to analyse the effect of temperature on the cluster properties. This has been approached in two ways. The first approach, summarized in

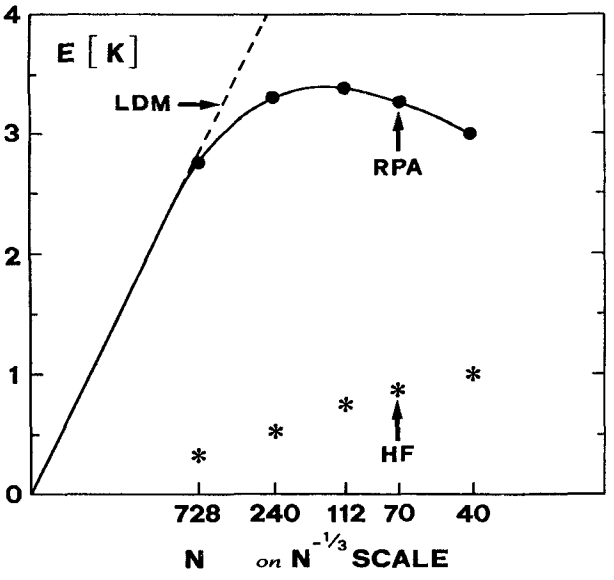

(*a*)

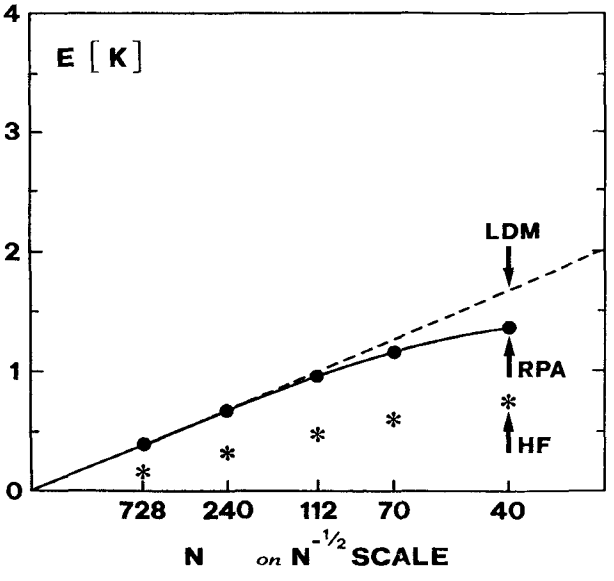

(*b*)

Figure 11. RPA excitation energies for He_N as a function of size N for (*a*) the $l=0$ compression mode and (*b*) the $l=2$ surface mode: (– – –), the LDM predictions; (*), Hartree–Fock (HF) results. (From Casas and Stringari 1990.)

§ 5.1 below, is to use statistical models built upon the classical LDM excitations. The second approach is to make a microscopic calculation of the thermal density matrix, using path integral techniques, and then to use this to evaluate thermal averages of interest. Path integral calculations for quantum clusters are described in § 5.2.

5.1. *Statistical descriptions*

This approach has been adopted by Stringari and co-workers to study several thermal properties of both ^4He_N and ^3He_N. Brink and Stringari (1990) use an LDM estimate of about 300 surface vibrational states below the first $L=0$, monopole compression mode for a cluster with $n=10^6$ atoms (Stringari 1991) as justification for building a model of the density of states of ^4He_N based only upon the surface vibrational modes. The results of § 4 indicate that this approximation would probably not be valid within a quantum treatment because the compressional modes lie lower in energy. By analogy with the bulk, these quantized surface modes are referred to as 'ripplons', although the quantization here is that of a classical wave on a finite cluster. Employing the LDM excitation energies yields a density $\omega(E)$ of states for ^4He_N in the microcanonical ensemble:

$$\omega(E)=\frac{1}{E^{5/7}}\exp(\alpha_s E^{4/3}N^{2/7}), \tag{5.1}$$

with α_s determined by the ^4He surface tension. For ^3He_N below its Fermi energy $T_f=4{\cdot}5$ K, $\omega(E)$ is approximated by the Bethe formula for a degenerate Fermi gas, which has quite a different energy and size dependence:

$$\omega(E)\approx\frac{1}{E}\exp\left[\left(\frac{\pi^2}{E_F}\right)^{1/2}(EN)^{1/2}\right]. \tag{5.2}$$

These densities of states can be used to derive heat capacities, and the evaporation and hence cooling rate of the clusters, using the Weisskopf evaporation formula

$$\frac{dN}{dt}=g\frac{\sigma}{\pi^2}m\int_0^{E-E_0}d\varepsilon\frac{\omega_{N-1}(E-E_0-\varepsilon)\varepsilon}{\omega_N(E)}, \tag{5.3}$$

where σ is the collision cross-section of an atom with an $N-1$ cluster, approximated by the classical value πR^2 with R the cluster radius, and g is the spin degeneracy of the evaporated particle. This gives cooling rates of about $10^9\,s^{-1}$ at $T=1$ K, with the ^4He_N rate being somewhat higher than the ^3He_N rate. For large clusters the ^4He_N rates are predicted to be independent of size and result in a final temperature of about 0·3 K after a time $t\approx10^{-3}$ s, in agreement with other estimates of experimental temperatures (Buchenau *et al.* 1990).

Pitaevskii and Stringari (1990) have further considered the effect of surface vibrations ('ripplons') on the superfluid behaviour of ^4He_N clusters. A quantitative estimate of the extents of superfluidity in both macroscopic and finite systems may be obtained from the deviation of the moment of inertia I_Q from its rigid value I_{rig}. This defines the normal (non-superfluid) fraction ρ_n, which is the complement of the superfluid fraction ρ_s in the bulk two-fluid picture, as

$$\frac{\rho_n}{\rho}=\frac{I_Q}{I_{rig}}, \tag{5.4}$$

with

$$\rho_n=\rho-\rho_s. \tag{5.5}$$

The quantum-mechanical moment I_Q, of inertia, can be defined in terms of the response to slow rotation about an axis passing through the centre of mass:

$$I_Q = \left(\frac{\partial \langle L_z \rangle_\omega}{\partial \omega} \right)_{\omega = 0}. \tag{5.6}$$

The angular brackets indicate a thermal average over all states populated at temperature T, and the zz component of I_Q is understood. For a spherical system, $I_{rig} = \frac{2}{3} MN \langle r^2 \rangle$. Explicit calculation including only the LDM surface states yields a low-temperature approximation for the normal density:

$$\frac{\rho_n}{\rho} = \frac{50}{27} \frac{1}{m_{He} r_0^2} \left(\frac{3 m_{He}}{4\pi\sigma} \right)^{4/3} \Gamma(\tfrac{5}{3}) \zeta(\tfrac{5}{3}) T^{5/3} N^{-1/3}, \tag{5.7}$$

which has a different temperature dependence from the bulk result (Wilks 1967)

$$\frac{\rho_n}{\rho} = \frac{2}{45} \frac{\pi^2}{\rho m_{He} c^5} T^4. \tag{5.8}$$

Figure 12 *a* compares the normal fraction as a function of temperature for two different cluster sizes, with the bulk behaviour. The superfluid component is seen to be depressed in the finite systems relative to the bulk, just as was seen in the simpler calculations of the zero-momentum component in a confined gas of non-interacting bosons (Krishna and Whaley 1991b). This is also seen in the path integral results discussed in § 5.2. Pitaevskii and Stringari (1990) have additionally considered the dependence of ρ_n on the rotation frequency and predict that, at a critical frequency

$$\omega_{cr} = 5{\cdot}1 N^{-1/2} \text{ K}, \tag{5.9}$$

there will be a condensation of surface phonons, accompanied by a permanent deformation and destruction of superfluidity.

5.2. *Path integral studies*

The first path integral calculations for quantum clusters were carried out by Cleveland *et al.* (1989), who made path integral molecular dynamics simulations for clusters of ^4He_N ($N = 57$, 120 and 270) at $T = 3$ K, with exchange effects neglected. Bulk studies have shown that exchange has little noticeable effect on structural or dynamical quantities above $T \approx 2$ K (Ceperley and Pollock 1986), and omitting this greatly simplifies path integral computations. Since the clusters can evaporate at finite temperatures, the calculations were carried out in a confining spherical box and resulted in an equilibrium between a central liquid region which was defined to constitute the cluster, and a surrounding vapour region of lower density. This gives rise to some ambiguities, as discussed by Scharf *et al.* (1992a). Cleveland *et al.* (1989) computed thermal averages of structural and energy properties for the liquid clusters. The results are generally comparable with the $T = 0$ QMC studies, with radial density distributions being more diffuse and the clusters being energetically more weakly bound than at $T = 0$. An interesting structural correlation here is that the transition from pachydermous ($\delta\rho/\delta\rho_0 < 0$) to leptodermous ($\delta\rho/\delta\rho_0 > 0$) behaviour mentioned in § 3.4, is moved to higher N at finite temperatures, reflecting the increased diffuseness.

Path integral Monte Carlo calculations for ^4He_N which incorporated full quantum exchange were subsequently carried out by Sindzingre *et al.* (1989). These workers developed two path integral estimators for the deviation of the quantum-mechanical

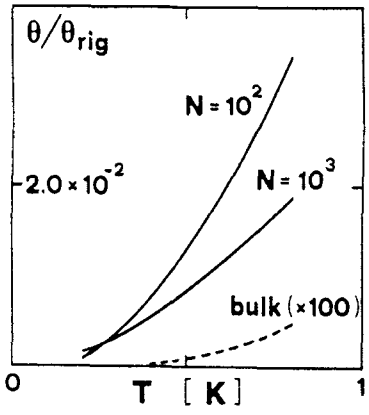

(a)

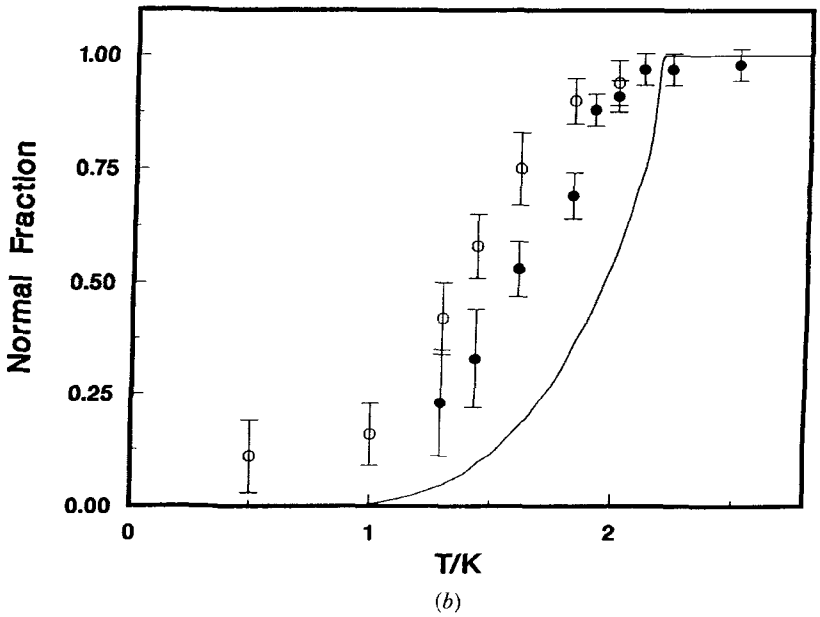

(b)

Figure 12. (*a*) Normal fraction in He_N as a function of T calculated from the LDM of surface excitations for $N=100$ and $N=1000$. (From Pitaevskii and Stringari (1990.) (*b*) Normal fraction in He_N as a function of T calculated from path integral studies for $N=64$ (○) and $N=128$ (●). (From Sindzingre *et al.* 1989.)

moment I_Q of inertia (equation 5.6) from its classical value. The first is the expectation value of the square of the surface area enclosed by the Feynman paths projected on to a plane perpendicular to the rotation axis. The second, more direct estimate is the probability that the projection of the angular momentum L on the axis has the value nh. These averages require the path integral representation of the density matrix, including summations over all particle permutations, and this is evaluated using a generalized Metropolis sampling algorithm. As a result of incorporating particle exchange, these become extremely time-consuming calculations at low temperatures (e.g. 200 central processing unit h on an IBM 3090/200 E with attached vector processors at $T=0{\cdot}5$ K).

These workers adjusted the size of the confining spherical box to avoid having any atoms in the vapour. Figure 12 *b* shows the calculated normal fluid fraction as a function of temperature for two different cluster sizes: $N=64$ and 128. The depression in superfluid component relative to the bulk is again apparent, just as in the LDM-derived result of Pitaevskii and Stringari (1990) (figure 12 *a*). It also appears that the superfluid transition temperature which corresponds to the onset of a decrease in ρ_n, is displaced to a lower temperature. This is confirmed by calculation of the heat capacities, which show rounded peaks displaced to lower temperatures as N decreases (Sindzingre *et al.* 1989), in accordance with the predictions of finite-size scaling (Ginzburg and Sobyanin 1976). These observations of finite superfluid fractions in finite-temperature calculations for clusters as small as $N=64$ are in good agreement with the estimate of a minimum size $N\approx 70$ for superfluidity made from the scaling of the excitation spectrum (§ 4.2) (Krishna and Whaley 1990a, b).

In the Feynman path integral representation, superfluidity is related to the occurrence of long paths which involve several permuting atoms (Pollock and Ceperley 1987). Sindzingre *et al.* (1989) used the probability that an atom is part of a permutation cycle involving several (six) atoms as a measure of superfluidity to analyse the spatial dependence of the superfluid density. They found that the superfluid density does drop to zero at the cluster surface, as expected from bulk considerations (Wilks 1967), but is nevertheless large near the surface region. Sindzingre *et al.* (1991) have also used this criterion to examine the propensity for superfluidity in small clusters of p-$(H_2)_N$. For $N=33$ the fraction remains low over the entire temperature range studied, 10–1 K. For smaller N, the fraction of the radial density profile due to such permutation cycles increases significantly as the temperature decreases. The behaviour of this fraction with decreasing N at a given temperature might be expected to depend both on the competing effects of more liquid-like behaviour associated with a lower melting point and, by analogy with ^4He_N, on a minimum size requirement. While too few clusters were studied to clarify this, it was noted that $N=13$ had a lower such fraction than $N=18$, although this could also be associated with the highly stable icosahedral structure at this size. The size dependence of this fraction is generally consistent with the path integral estimate of the normal fluid fraction for these clusters, which decreases to values significantly below unity for $N=13$ and 18 while, for $N=33$, only a very small decrease is seen. Detailed analysis of the difference between $N=13$ and 18 is not possible however, because of the large statistical error in this quantity. It is nevertheless noticeable that the decrease in the normal fraction for a given size starts at a higher temperature than found for the ^4He_N clusters, indicating a higher superfluid transition temperature for H_2. This is entirely consistent with the predictions made on the basis of the Bose–Einstein condensation temperature (§ 1) (Ginzburg and Sobyanin 1976).

More extensive structural studies have been carried out for molecular hydrogen clusters by the path integral Monte Carlo technique without exchange (Scharf *et al.* 1992a, b). As noted above, this greatly simplifies the calculations and allows a more detailed and better converged analysis. Any quantum effects are then entirely due to the zero-point motion which accounts for residual positional permutations of particles seen at $T\approx 2$ K. However, the omission of exchange for H_2 is only negligible above $T\approx 2{\cdot}5$ K (Sindzingre *et al.* 1991), and so the conclusions of these studies are restricted to this and higher temperatures. All calculations are carried out with the spherical part of the H_2–H_2 potential only. Scharf *et al.* (1992a, b) use averaged quantities such as the pair distribution function $g(r)$, radial density profiles and average r.m.s. displacements $\delta_{r.m.s.}$ together with examination of individual contributing structures, to characterize

the p-$(H_2)_N$ clusters as quantum liquids for $T < 6$ K, above which they are unstable with respect to evaporation. This characterization is based primarily upon the magnitude of $\delta_{r.m.s.}$ (Scharf *et al.* (1992b) use $\delta_{r.m.s.} > 15\%$ for a quantum liquid). The quantum-liquid phase exhibits many spatial permutations involving three or more molecules even without exchange permutations. Most interesting is the systematic observation of instantaneous high-symmetry fivefold structures at $T \approx 2{\cdot}5$ K, which are based upon pentagonal bipyramidal and icosahedral cores. These well ordered configurations appear in all size clusters but do not dominate the long-time average structures of any cluster size. As noted in § 3.2, a large contribution of structures with approximate fivefold symmetry is also observed in the $T = 0$ structures of $(H_2)_7$ (pentagonal bipyramid), although these only constitute a fraction of the extensively delocalized quantum liquid ground state (McMahon *et al.* 1993). Scharf *et al.* (1992a) note that these high-symmetry structures appear to be stabilized by the presence of additional outer shells, which lead to smaller fluctuations and increasingly rigid cores for larger N. This may be the origin of the reduced superfluidity in $N = 33$ (Sindzingre *et al.* 1991) and can be regarded as causing a gradual transition from a quantum liquid to a quantum solid phase as a function of N, with the solidification proceeding from the cluster centre outwards.

In contrast with the behaviour of p-$(H_2)_N$, the isotopic analogues o-$(D_2)_N$ appear much more localized and show a decrease in $\delta_{r.m.s.}$ from values of about 0·3 at $T = 6$ K, to values less than 0·1 below $T = 4$ K (Scharf *et al.* 1992b). This is interpreted as indicating a phase transition from a quantum liquid to a quantum solid, by analogy with previous quantum and classical simulations for Lennard-Jones clusters (Beck *et al.* 1989).

Scharf *et al.* (1993) have recently extended the path integral Monte Carlo method to the study of impurities in molecular hydrogen clusters and have analysed the structure of lithium impurities in p-$(H_2)_N$. These studies indicate that the lithium lowers the range of stability of the clusters, which now evaporate H_2 at lower temperatures. The lithium atom is situated either outside the cluster or at the cluster surface and has little effect on the interior liquid–solid behaviour. The spectral properties of these impurities are of prime interest, just as with the molecular impurities discussed in §§ 2 and 3. Scharf *et al.* (1993) find that the ionization potential of lithium is red shifted in the clusters, and that the absorption spectra are distorted and blue shifted, with both shifts increasing as the cluster size increases.

5.3. *Scattering of quantum clusters*

Despite the experimental attention focused on scattering studies of helium clusters, little theoretical work has addressed either scattering or absorption of foreign particles by quantum clusters. This reflects the lack of knowledge of the cluster excitations and should change as these become better characterized with the techniques described in previous sections. The only theoretical study of scattering from helium clusters to date was performed by Eichenauer *et al.* (1988) for helium scattering from helium clusters, employing the classical macroscopic LDM for the cluster surface excitations (§ 4.1). Using a distorted-wave Born approximation and neglecting exchange between the incoming helium and the cluster atoms, they calculated vibrationally inelastic cross-sections for surface excitations of clusters containing between 10 and 1000 atoms. These are of order 100 Å^2, decreasing at higher energies, and they show pronounced oscillations. Some oscillations were assigned to diffraction interference effects and others to orbiting resonances. Eichenauer *et al.* (1988) also investigated the elastic and

absorption cross-sections for several absorption models: hard- and transparent-core clusters, completely absorptive and optical potential models. These cross-sections are larger, typically 10^3 or 10^4 Å^2, and also show oscillatory behaviour as a function of energy, although to a lesser extent than the vibrational cross-sections. Generally these cross-sections were found to depend only weakly upon cluster size N, in the range $N = 100$–1000.

A major problem in such scattering studies is the projectile–cluster interaction potential. For very large clusters, direct summation over all cluster components is impractical, and various approximations have therefore been developed. The study of Eichenauer *et al.* (1988) used two different models. The first is a hard-core model in which the helium-cluster potential is obtained by integrating over a sphere of uniformly distributed Lennard-Jones 6–12 potentials. This ignores the cluster internal structure. The second model matches a long-range attractive term, obtained by integrating over a sphere of homogeneously distributed $-C_6/r^6$ potentials, to a constant negative potential in the cluster interior. This transparent-core model therefore also neglects the cluster structure. It is clear that either explicit summation or more realistic potential models are required to deal with internal cluster excitations such as compressional modes.

Scattering of high-energy particles will also involve dissociation of the excited clusters. This is the case with electron scattering at energies of about 20eV (Martini *et al.* 1991) as well as at the higher energies (about 50 eV) used in mass spectrometer sources (Buchenau *et al.* 1990). Electron scattering has yielded estimates of the electronic surface barrier potential (Martini *et al.* 1991). The contributions from charge-transfer processes and the proliferation of electronic dynamical channels involving metastable species causes the interpretation of such experiments to present a considerable challenge to theory. A further challenge, which is also increasingly becoming an experimental reality, is the scattering of atoms and molecules from clusters to which other foreign species have already been attached. Understanding the scattering behaviour from the pure clusters is a prerequisite for this more complex dynamical situation in which there may be strong effects of the quantum 'solvent' on the molecular collision dynamics.

6. Conclusions

In this review we have summarized the theoretical studies made of quantum clusters in the past 15 years, giving also a brief review of the experimental advances in this field. Considerable progress in understanding pure clusters of helium has been achieved, and a significant start has been made on the study of foreign molecules attached to helium clusters. All these studies, with some modifications, apply also to clusters of molecular hydrogen, which have not received as much attention. The current focus of both experimental and theoretical efforts on spectroscopic studies of attached molecular species promises to yield useful information on the structural and, eventually, also on the dynamical properties of these clusters. However, it is clear that much more analysis and computational study is required in order to provide adequate explanation of existing experimental studies of molecular pick-ups. The study of scattering and dissociation processes has barely been addressed. Another significant area requiring new theoretical input is that of electronic excitations of these clusters. Electron bombardment and the subsequent energy transfer and dissociation processes play an important part in mass spectrometry studies and yet are poorly understood at best. Synchrotron sources have recently been utilized to obtain fluorescence spectra of He_N

which show very different behaviour from the clusters of the heavier rare gases (Joppien *et al.* 1993). More generally, the structural changes resulting from the attachment of ionic species to the clusters need to be considered, particularly since these are usually easier to study experimentally than neutrals. Theoretically, it will be necessary to take into account the strong localization and polarization forces of ionic species, which are usually associated with a 'snowball' type of structure in bulk helium (Benneman and Ketterson 1976).

With these challenges still ahead, the study of quantum clusters clearly offers many possibilities for the investigation of chemical and physical properties of very weakly bound atomic and molecular aggregates. Many of these will be addressable by the methods summarized here.

Acknowledgments

Our work on helium clusters described here was supported by the Office of Naval Research, under Grant No. ONR N00014-89-J-1755. Additional support is gratefully acknowledged from National Science Foundation (Grant No. CHE-8907423) and from the Petroleum Research Fund (Grant No. 21435-AC5/6). I would like to thank Dr Robert Barnett for a careful reading of the manuscript. K.B.W. was an Alfred P. Sloan Research Fellow, 1991–1993.

References

AZIZ, R. A., MCCOURT, F. R. W., and WONG, C. C. K., 1987, *Molec. Phys.*, **61**, 1487.
AZIZ, R. A., NAIN, V. P. S., CARLEY, J. S., TAYLOR, W. L., and MCCONVILLE, G. T., 1979, *J. chem. Phys.*, **70**, 4330.
BACIC, Z., KENNEDY-MANZUIK, M., MOSKOWITZ, J. W., and SCHMIDT, K. E., 1992, *J. chem. Phys.*, **97**, 6472.
BARNETT, R. N., CAHN, B., and WHALEY, K. B., 1993 (in preparation).
BARNETT, R. N., and WHALEY, K. B., 1992, *J. chem. Phys.*, **96**, 2953; 1993a, *Phys. Rev.* A, **47**, 4082; 1993b, *J. chem. Phys.* (in press).
BARTLETT, R. J., 1989, *J. phys. Chem.*, **93**, 1697.
BECK, T. L., DOLL, J. D., and FREEMAN, D. L., 1989, *J. chem. Phys.*, **90**, 5651.
BECKER, E. W., KLINGELHOFER, R., and LOHSE, P., 1961, *Z. Naturf.* (a), **16**, 1259.
BENNEMAN, K. H., and KETTERSON, J. B. (eds), 1976, *The Physics of Liquid and Solid Helium*, Part I (New York: Wiley).
BERTSCH, G. F., and TSAI, S. F., 1975, *Phys. Rep.* C, **18**, 126.
BIJL, A., 1940, *Physica*, **7**, 896.
BOHR, A., and MOTTELSON, B. R., 1975, *Nuclear Structure*, Vol. II (New York: Benjamin).
BOREL, J.-P., 1981, *Surf. Sci.*, **106**, 1.
BREWER, D. F., RAJENDRA, J., SHARMA, N., and THOMSON, A. L., 1990, *Physica* B, **165R166**, 569.
BRINK, D. M., and STRINGARI, S., 1990, *Z. Phys.* D, **15**, 257.
BUCHANAU, H., GOETTING, R., MINUTH, R., SCHEIDEMAN, A., and TOENNIES, J. P., 1985, *Flow of Real Fluids*, Lecture Notes in Physics, Vol. 235, edited by G. E. A. Meier and F. Obermeier (Berlin: Springer), p. 157; 1986, *Proceedings of the 15th Symposium on Rarefied Gas Dynamics*, Vol. II, edited by V. Boffi, and C. Cergignani (Stuttgart: Teubner), p. 197.
BUCHENAU, H., KNUTH, E. L., NORTHBY, J., TOENNIES, J. P., and WINKLER, C., 1990, *J. chem. Phys.*, **91**, 6875.
BUCK, V., HUISKEN, F., KOHLHASE, A., OTTEN, D., and SCHAEFER, J., 1983, *J. chem. Phys.*, **78**, 4439.
BUFFAT, PH., and BOREL, J.-P., 1976, *Phys. Rev.* A, **13**, 2287.
CASAS, M., and STINGARI, S., 1990, *J. low temp. Phys.*, **79**, 135.
CASTRO, T., REIFENBURGER, R., CHOI, E., and ANDRES, R. P., 1990, *Phys. Rev.* B, **42**, 8548.
CEPERLEY, D. M., and POLLOCK, E. L., 1986, *Phys. Rev. Lett.*, **56**, 351.
CHANDRASEKAR, S., 1965, *Proc. R. Soc.* A, **268**, 1.
CHARTRAND, D. J., SHELLEY, J. C., and LEROY, R. J., 1991, *J. phys. Chem.*, **95**, 8310.
CHIN, S. A., and KROSTSCHECK, E., 1990, *Phys. Rev. Lett.*, **65**, 1658; 1992, *Phys. Rev.* B, **45**, 852.

CLEVELAND, C. L., LANDMAN, U., and BARNETT, R. N., 1989, *Phys. Rev.* B, **39,** 117.
DALFOVO, F., 1989, *Z. Phys.* D, **14,** 263.
DONIACH, S., and SONDHEIMER, E. H., 1974, *Green's Function for Solid State Physicists* (Reading, MA: Benjamin–Cummings).
EICHENAUER, D., and LEROY, R. J., 1988, *J. chem. Phys.*, **88,** 2898.
EICHENAUER, D., SCHEIDEMANN, A., and TOENNIES, J. P., 1988, *Z. Phys.* D, **8,** 295.
ERCOLESSI, F., ANDREONI, W., and TOSATTI, E., 1991, *Phys. Rev. Lett.*, **66,** 911.
FEYNMAN, R. P., 1954, *Phys. Rev.*, **94,** 262.
FEYNMAN, R. P., and COHEN, M., 1957, *Phys. Rev.*, **107,** 13.
GARCIA-VELA, A., VILLARREAL, P., and DELGARDO-BARRIO, G., 1990, *J. chem. Phys.*, **92,** 6504.
GINZBURG, V. L., and SOBYANIN, A. A., 1972, *JETP Lett.*, **15,** 242; 1976, *Usp. fiz. Nauk.*, **120,** 153 (Engl. Transl., 1976, *Soviet Phys. Usp.*, **19,** 773.
GORDON, E. B., KHMELKENKO, V. V., PELMENEV, A. A., POPOV, E. A., and PUGACHEV, O. F., 1989, *Chem. Phys. Lett.*, **155,** 301.
GORDON, E. B., KHMELENKO, V. V., PELMENEV, A. A., POPOV, E. A., PUGACHEV, O. F., and SHESTAKOV, A. F., 1993, *Chem. Phys.*, **170,** 411.
GOYAL, S., SCHUTT, D. L., and SCOLES, G., 1992a, *Phys. Rev. Lett.*, **69,** 933.
GOYAL, S., SCHUTT, D. L., SCOLES, G., and ROBINSON, G. N., 1992b, *Chem. Phys. Lett.*, **196,** 123.
GSPANN, J., 1981a, *Surf. Sci.*, **106,** 219; 1981b, *Physica* B, **108,** 1309; 1982, *Physics of Electronic and Atomic Collisions*, edited by S. Datz (Amsterdam: North-Holland); 1991, *Physica* B, **169,** 519.
GSPANN, J., and RIES, R., 1985, *Surf. Sci.*, **156,** 195; 1986, Kernforschungszentrum Karlsruhe GmbH Report No. KfK 4156.
GSPANN, J., and VOLLMAR, H., 1978, *J. Phys., Paris*, **39,** C6–330; 1980, *J. chem. Phys.*, **73,** 1657.
HELMBRECHT, U., and ZABOLITZKY, J. G., 1984, *Monte Carlo Methods in Quantum Problems*, edited by M. H. Kalos (Dordrecht: Reidel).
HORN, T. R., GERBER, R. B., and RATNER, M. A., 1989, *J. chem. Phys.*, **91,** 1813.
JIANG, T., and NORTHBY, J. A., 1992, *Phys. Rev. Lett.*, **68,** 2620.
JOPPIEN, M., MÜLLER, R., and MÖLLER, T., 1993, *Z. Phys.* D (in press).
KALOS, M. E., LEE, M. A., WHITLOCK, P. A., and CHESTER, G. V., 1981, *Phy. Rev.* B, **24,** 115.
KALOS, M. H., LEVEQUE, D., and VERLET, L., 1974, *Phys. Rev.* A, **9,** 2178.
KNUTH, E. L., SCHILLING, B., and TOENNIES, J. P., *17th International Symposium of Rarefied Gas Dynamics*, p. 1035, Edited by A. E. Beylich, VCH Weinheim 1991.
KOSLOFF, R., HAMMERICH, A., and RATNER, M. A., 1987, *Large Finite Systems*, edited by J. Jortner, A. Pullman and B. Pullman (Dordrecht: Reidel), p. 53.
KRISHNA, M. V., and WHALEY, K. B., 1988, *Phys. Rev.* B, **38,** 11389; 1990a, *Phys. Rev. Lett.*, **54,** 1126; 1990b, *J. chem. Phys.*, **93,** 746; 1990c, *Mod. Phys. Lett.* B, **14,** 895; 1990d, *J. chem. Phys.*, **93,** 6738; 1990a, *Z. Phys.* D, **20,** 223; 1990b, *On Clusters and Clustering: from Atoms to Fractals*, edited by P. J. Reynolds (Amsterdam: North-Holland).
KROTSCHECK, E., STRINGARI, S., and TREINER, J., 1987, *Phys. Rev.* B, **35,** 4754.
KURTEN, K. E., and RISTIG, M. L., 1985, *Phys. Rev.* B, **31,** 1346.
LEWART, D. S., PANDHARIPANDE, V. R., and PIEPER, S. C., 1988, *Phys. Rev.* B, **37,** 4950.
LEWERENZ, M., SCHILLING, B., and TOENNIES, J. P., 1993, *Chem. Phys. Lett.*, **206,** 381.
LIU, K. F., and VAN GIAI, N., 1976, *Phys. Lett.* B, **65,** 23.
MARIS, H. J., SEIDEL, G. M., and HUBER, T. E., 1983, *J. low Temp. Phys.*, **51,** 471.
MARTINI, K., TOENNIES, J. P., and WINKLER, C., 1991, *Chem. Phys. Lett.*, **178,** 429.
MCMAHON, M. A., BARNETT, R. N., and WHALEY, K. B., 1993, *J. chem. Phys.* (in press).
MCMAHON, M. A., and WHALEY, K. B., 1993, *J. chem. Phys.*, (submitted).
MELZER, R., and ZABOLITSKY, J. G., 1984, *J. Phys.* A, **17,** L565.
PACK, R. T., PIPER, E., PFEFFER, G. A., and TOENNIES, J. P., 1984, *J. chem. Phys.*, **80,** 4940.
PANDHARIPANDE, V. R., PIEPER, S. C., and WIRINGA, R. B., 1986, *Phys. Rev.* B, **34,** 4571.
PANDHARIPANDE, V. R., ZABOLITZKY, J. G., PIEPER, S. C., WIRINGA, R. B., and HELMBRECHT, U., 1983, *Phys. Rev. Lett.*, **50,** 1676.
PIEPER, S. C., WIRINGA, R. B., and PANDHARIPANDE, V. R., 1985, *Phys. Rev.* B, **32,** 3341.
PITAEVSKII, L. P., 1957, *Soviet Phys. JETP*, **4,** 439.
PITAEVSKII, L. P., and STRINGARI, S., 1990, *Z. Phys.* D, **16,** 299.
POLLOCK, E. L., and CEPERLEY, D. M., 1987, *Phys. Rev.* B, **36,** 8343.
RICK, S. W., and DOLL, J. D., 1992, *Chem. Phys. Lett.*, **188,** 149.

RICK, S. W., LEITNER, D. M., DOLL, J. D., FREEMAN, D. L., and FRANTZ, D. D., 1991a, *J. chem. Phys.*, **95,** 6658.
RICK, S. W., LYNCH, D. L., and DOLL, J. D., 1991b, *J. chem. Phys.*, **95,** 3506.
SCHARF, D., KLEIN, M. L., and MARTYNA, G. J., 1992a, *J. chem. Phys.*, **97,** 3590.
SCHARF, D., MARTYNA, G. J., and KLEIN, M. L., 1992b, *Chem. Phys. Lett.*, **197,** 231; 1993, *J. chem. Phys.* (in press).
SCHEIDEMANN, A., 1989, Ph.D. Thesis, Max-Planck Institut fuer Strömungs Forschung, Göttingen.
SCHEIDEMANN, A., SCHILLING, B., and TOENNIES, J. P., 1993, *J. phys. Chem.*, **97,** 2128.
SCHEIDEMANN, A., SCHILLING, B., TOENNIES, J. P., and NORTHBY, J. A., 1990a, *Physica* B, **165–166,** 135.
SCHEIDEMANN, A., TOENNIES, J. P., and NORTHBY, J. A., 1990b, *Phys. Rev. Lett.*, **64,** 1899.
SCHUTT, D. L., 1992, Ph.D. Thesis, Princeton.
SCHWARTZ, K. W., 1975, *Adv. chem. Phys.*, **33,** 1.
SHENG, P., COHEN, R. W., and SCHRIEFFER, J. R., 1981, *J. Phys.* C, **14,** L565.
SINDZINGRE, P., KLEIN, M. L., and CEPERLEY, D. M., 1989, *Phy. Rev. Lett.*, **63,** 1601; 1991, *Ibid.*, **67,** 1871.
STEPHENS, P. W., and KING, J. G., 1983, *Phys. Rev. Lett.*, **51,** 1538.
STRINGARI, S., and TREINER, J., 1987, *J. chem. Phys.*, **87,** 5021.
STRINGARI, S., 1991, *Z. Phys. D*, **20,** 219.
SYSKAKIS, E. G., FUJI, Y., POBELL, F., and SCHROEDER, H., 1990, *Physica* B, **165,** 789.
SYSKAKIS, E. G., POBELL, F., and ULLMAIER, H., 1985, *Phys. Rev. Lett.*, **55,** 2964.
TILLEY, D. R., and TILLEY, J., 1986, *Superfluidity and Superconductivity* (Bristol: Adam Hilger).
USMANI, N., FANTONI, S., and PANDHARIPANDE, V. R., 1982, *Phys. Rev.* B, **26,** 6123.
VAN DEURSEN, A. J. P., and REUSS, J., 1975, *J. chem. Phys.*, **63,** 4559.
WEAST, R. C., (ed.), 1981, *CRC Handbook of Chemistry and Physics* (West Palm Beach, FL: CRC Press).
WHITLOCK, P. A., CEPERLEY, D. M., CHESTER, G. V., and KALOS, M. H., 1979, *Phys. Rev.* B, **19,** 5598.
WILKS, J., 1967, *Properties of Liquid and Solid Helium* (Oxford: Clarendon).